
Application of Image-Based Remote Sensing to Irrigated Agriculture

M. Susan Moran

Southwest Watershed Research Center
USDA-ARS
Tucson, Arizona

Stephen J. Maas

Texas Tech University
Lubbock, Texas

Vern C. Vanderbilt

Ames Research Center
NASA
Moffett Field, California

Edward M. Barnes

Cotton Incorporated
Cary, North Carolina

Scott N. Miller

Rangeland Ecology and Watershed Management
University of Wyoming
Laramie, Wyoming

Thomas R. Clarke

U.S. Water Conservation Laboratory
USDA-ARS
Phoenix, Arizona

12.1 INTRODUCTION

The U.S. Department of Agriculture (USDA) estimated that in 1998 there were over 21 million hectares of irrigated agriculture in the United States and over 271 million hectares of irrigated agriculture in the world. A growing population throughout the United States and the world depends directly on irrigated agriculture for both food and employment. Irrigated agriculture provides higher and more dependable crop production on a per unit area basis than that of dryland systems, thus reducing the amount of land converted from natural ecosystems to meet the world's food and fiber demands. Ironically, this growing dependence on irrigated agriculture has been accompanied by a growing perception that irrigation is economically unsound, due to the current low prices for many irrigated crops and the high cost of irrigation water and services. Irrigation is also perceived to be detrimental to the environment, due to waterlogging, soil salinity, and percolation of agricultural chemicals into soils and the underlying water table. Public pressure associated with these perceptions, along with the growing importance of water trading in recent years, has encouraged producers to seek better means to manage water resources.

Managers of irrigated lands are seeking an information-based crop management system that will improve agricultural water use efficiency, enhance crop productivity, and reduce the potential detrimental impact of irrigated agriculture on the environment. Some innovative farm managers are looking to remote sensing for accurate, spatially distributed information about crop and soil conditions that can be used to schedule timing and amount of crop irrigations and plan associated agricultural activities. Such users view remote sensing as simply another source of information that differs in accuracy, sampling density, and turnaround time from the available conventional sources of information, such as neutron probes for measuring soil moisture, soil penetrometers for finding claypan, and petiole samples for determining plant nitrogen status. That is, remote sensing is seen as part of a continuum of available tools rather than a discrete departure from conventional information sources (Swinton and Jones, 1998) (Figure 12.1).

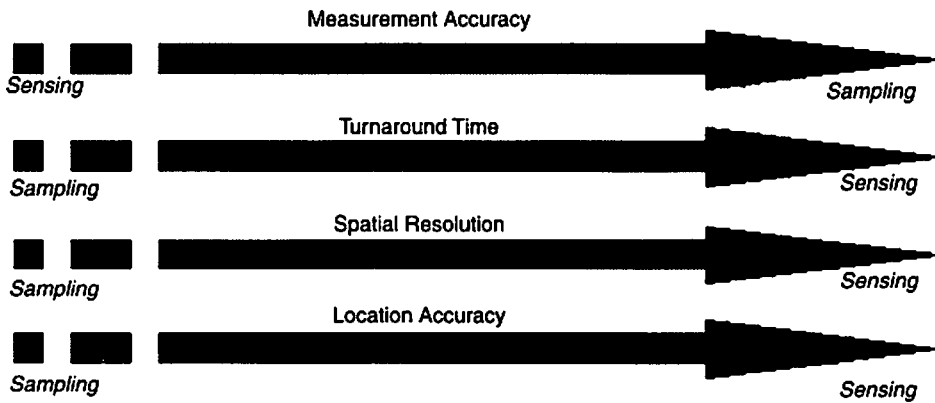


Figure 12.1 Conceptual model of remote sensing as a continuum of conventional farm management tools, where sensing differs from sampling in measurement accuracy, turnaround time, spatial resolution, and location accuracy. (After Swinton and Jones, 1998.)

The viewpoint that remote sensing is part of a "toolbox" for agricultural management has been fostered further by concurrent advances in related technologies. These include variable-rate technology (VRT), global positioning systems (GPSs) and geographic information systems (GISs). Variable-rate technology (VRT) applies production inputs at rates appropriate to soil and plant conditions within fields. Variable-rate systems have been demonstrated for several materials, including herbicide (Mortensen et al., 1995), fertilizer (Schueller, 1992; Ferguson et al., 1995), insecticide (Fleischer et al., 1997), and seeds. Advances in GPS technology have provided the moderately priced, accurate positioning system necessary for field implementation of VRT (Palmer, 1995). These advances in location technology have been combined with the ubiquitous use of GISs by farm managers in the most advanced systems for precision farming (Usery et al., 1995). For example, Hanson et al. (1995) described a herbicide application system mounted on a tractor with a GPS guidance system that was linked to a digital weed map, allowing only weed-infested areas of a field to be sprayed. The weak link in such systems is the availability of such maps of weeds, insect infestations, crop nutrient deficiencies, and other crop and soil conditions. Remotely sensed images obtained with aircraft- and satellite-based sensors have the potential to provide such maps for an entire field, not just sample sites, within the time and space requirements of crop management applications.

The community sentiment that remote sensing can meet information requirements for crop and soil management is based largely on results of remote sensing research conducted over the past 30 years. In the late 1970s and early 1980s, a great research effort was focused on the use of multispectral images for crop inventory and crop production. The Large Area Crop Inventory Experiment (LACIE) demonstrated the feasibility of utilizing satellite-based multispectral data for estimating wheat production (MacDonald and Hall, 1980) based on techniques that are still in use by crop production forecasters in the USDA Foreign Agricultural Service. The AgRISTARS program conducted by the USDA, NASA, and NOAA extended this methodology to include other crops and regions and expanded the research to encompass larger agricultural issues. The LACIE and AgRISTARS programs not only produced robust methods for regional crop identification and condition assessment, but also defined the physics of relations between spectral measurements and biophysical properties of crop canopies and soils. It was widely recognized that this basic scientific and technical knowledge had great potential to be used by farmers for making day-to-day management decisions.

Jackson (1984) evaluated current and future remote sensing systems for use in farm management. His 20-year vision for an ideal system included a fleet of autonomous satellites providing frequent high-resolution data with quick turnaround and delivery to users. This vision may soon become reality with the recent and planned launches of several commercial satellites that are designed to provide multispectral images with three-day repeat coverage, 1 to 4 m spatial resolution, and delivery to users within 15 minutes of the time of acquisition (Moran et al., 1997b). The synergy of such an imaging system with the scientific algorithms and models developed over the past 30 years could provide detailed crop and soil information to farm managers and crop consultants at a finer temporal and spatial scale than ever before.

This watershed of technology and scientific advances has led to partnerships between agricultural producers and remote sensing experts to define the information needs of producers and better direct remote sensing research toward satisfying these

needs using remote sensing products. A good example of such an initiative is the Ag20/20 group, where the Ag20/20 acronym represents a "clear vision" of agriculture. The formation of this group was facilitated by a 1998 Memorandum of Understanding between USDA and NASA to encourage cooperation between the groups for the benefit of U.S. agriculture. Members of the National Corn Growers Association, National Cotton Council, American Soybean Association, and National Association of Wheat Growers joined with NASA and USDA to form Ag20/20. The basic goals of Ag20/20 are to develop remote sensing-based crop production and management tools that will (1) increase U.S. farmers' profit margins, (2) reduce crop production risks, and (3) minimize environmental impacts associated with agricultural production.

The first step in the Ag20/20 program was to define grower information needs and baselines for information product development. This was accomplished through a series of meetings in 1999 in which commodity groups were asked to prioritize their top three information needs for agricultural management. The top priorities focused on nutrient, pesticide, and water management, while the second tier of priorities addressed a combination of factors ranging from crop yield, vigor, and quality to soil characterization and preparation (Table 12.1). Although defined primarily for U.S. production of corn, cotton, soybean, and wheat, these information needs are directly applicable to irrigated agriculture in general, and thus can be extended to orchards and vineyards. As such, these information needs were used to organize this chapter.

TABLE 12.1 Grower Information Needs Defined by Ag20/20 Group for Irrigated and Dryland Corn, Cotton, Soybean, and Wheat^a

<u>Priorities Common to All Four Crops</u>	
Irrigation/water information	Efficient management and scheduling of irrigation for optimal crop production
Nutrient application	Optimal allocation of fertilizer to maximize yields and minimize costs
Weed scouting/herbicide application	Early detection of weeds to prescribe herbicides in a spatially variable manner
Insect scouting/insecticide application	Routine detection of insect-prone areas to prescribe insecticides in a spatially variable manner
<u>Additional Top-Three Priorities</u>	
Crop yield	Development of tools to (1) increase yield and (2) predict/forecast yield for marketing decisions
Soil characterization	Extraction of accurate soils information for the delineation of sound management zones
Vigor/stress detection ^b	Detection of variations in crop health for variable-rate applications
Grain quality ^b	Characterization of grain-quality factors (oil, protein, etc.) for appropriate harvest and market decisions
Next-season preparation	Assessment of physical properties of fields after harvest to support planning or upcoming crop

^aAg20/20 members representing growers of each commodity were asked to define their top three information needs for agricultural management.

^bThese information needs were not addressed in this chapter.

Our primary objective in this chapter is to address the use of image-based remote sensing for irrigated agriculture. In the next section we present an overview of the physical plant and soil manifestations associated with water stress. Following that, potential applications of remote sensing and selected remote sensing product developments are reviewed for the information needs prioritized by Ag20/20 (Table 12.1). The chapter concludes with a summary of the current development stage of remote sensing for irrigated agriculture.

12.2 BACKGROUND

Numerous studies have shown that crop water stress has a direct effect on crop growth, development, and yield, and ultimately, on farmers' profits. The goal in managing the stress of crop species is not simply to keep plants alive during periods of water deficit, but to produce a profitable yield. To achieve this delicate balance between water use and crop yield, farm managers need an operational means to quantify plant water deficit and evaluate the effects of stress on a given crop species at any stage of development. In the following sections we present the plant manifestations of water stress that can be detected with the thermal-infrared (TIR) wavelengths and the visible, near-infrared (NIR), shortwave-infrared (SWIR), and synthetic aperture radar (SAR) wavelengths. The relevant optical properties of crop leaves and canopies are also included as a reference for discussions in the following sections.

12.2.1 Crop Water Stress and TIR Wavelengths

A commonly used measure of crop stress is the stress degree index (SDI) proposed by Hiler and Clark (1971). The SDI is based on a measure of the degree and duration of plant water deficit and the plant's susceptibility to a given water deficit:

$$SDI = \sum_n^{i=1} (SD_i \cdot CS_i) \quad (12.1)$$

where SD is the stress day factor, CS the crop susceptibility factor, and n represents the number of growth periods considered. SD is defined by the plant evaporation rate (E) and the potential evaporation rate (E_p), where

$$SD = 1 - \frac{E}{E_p} \quad (12.2)$$

CS represents the susceptibility of a crop to a given magnitude of SD and is a function of the species and stage of growth of the crop. Hiler and Clark (1971) suggested that CS be determined through field experiments with variable soil water conditions so that the natural environment was simulated as closely as possible.

For solution of equation (12.1), values of CS can be obtained for a variety of crops from a table compiled by Hiler and Clark (1971). However, SD must be evaluated *in situ* using meteorological measurements to estimate E_p and specialized

instrumentation to measure E . The specialized instruments commonly used to measure E (e.g., lysimeters, energy flux sensors, and gas exchange chambers) are generally too complex, labor intensive, or delicate for long-term field deployment, and the scale of measurement rarely matches the size and shape of agricultural fields. Thus, there has been interest in the use of remote sensing, in particular plant canopy temperature, to evaluate the spatial distribution and temporal dynamics of SD.

The link between studies of the physics of evaporation and the measurements of leaf temperatures was made by Monteith and Szeicz (1962) through their use of infrared thermometers (IRTs) to measure plant canopy temperatures. Based on energy balance considerations, they derived an expression relating the canopy-air temperature difference to net radiation, wind speed, vapor pressure gradient, and aerodynamic and canopy resistances, where

$$T_c - T_a = \frac{r_a(R_n - G)}{\rho C_p} \frac{\gamma(1 + r_c/r_a)}{\Delta + \gamma(1 + r_c/r_a)} - \frac{\text{VPD}}{\Delta + \gamma(1 + r_c/r_a)} \quad (12.3)$$

where

- T_c = canopy temperature (C or K)
- T_a = air temperature (C or K)
- r_a = aerodynamic resistance (s/m)
- R_n = net radiant heat flux density (W/m^2)
- G = soil heat flux density (W/m^2)
- Δ = slope of the saturated vapor pressure-temperature relation ($\text{kPa}/^\circ\text{C}$)
- ρ = volumetric heat capacity of air ($\text{J}/^\circ\text{C} \cdot \text{m}^3$)
- γ = psychrometric constant ($\text{kPa}/^\circ\text{C}$)
- r_c = canopy resistance to vapor transport (s/m)
- VPD = vapor pressure deficit of the air (kPa)

Equation 12.3, given in a slightly different form by Monteith and Szeicz (1962), was the basis for the theoretical development of a crop water stress index (CWSI), which is discussed in the next section. In the decade following this landmark work, infrared technology advanced rapidly, leading to the handheld, airborne, and satellite-based sensors and scanners that are available today (e.g., Figure 12.2).

An example of the distinctive variations in surface temperature in response to differential water treatments is presented in Figure 12.3 for a cotton field near Phoenix, Arizona. Boxes were drawn around plots with low-water treatments that had not been irrigated for six days, while the other plots were irrigated the previous day. In the low-water plots, 60% of plant-available water was depleted at the time of measurements. Average air temperature during the time of measurement was 32°C and the vapor pressure deficit was 2.0 kPa. The crop had reached canopy closure and had entered the boll formation growth stage about seven days earlier.

12.2.2 Crop Water Stress and Visible, NIR, SWIR, and SAR Wavelengths

To avoid the inherent difficulties associated with processing TIR measurements (see Moran, 2001), studies have focused on the use of other wavelengths to monitor

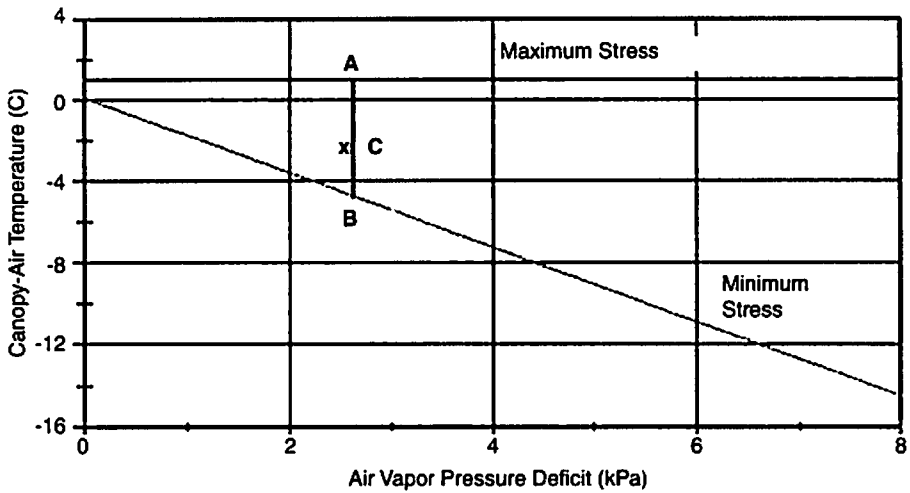


Figure 12.2 Canopy minus air temperature ($T_c - T_a$) versus vapor pressure deficit (VPD) for well-watered and maximally stressed alfalfa based on measurements at various sites across the United States. The CWSI is computed as the ratio of the distances CB and AB . (Data from Idso et al., 1981.)

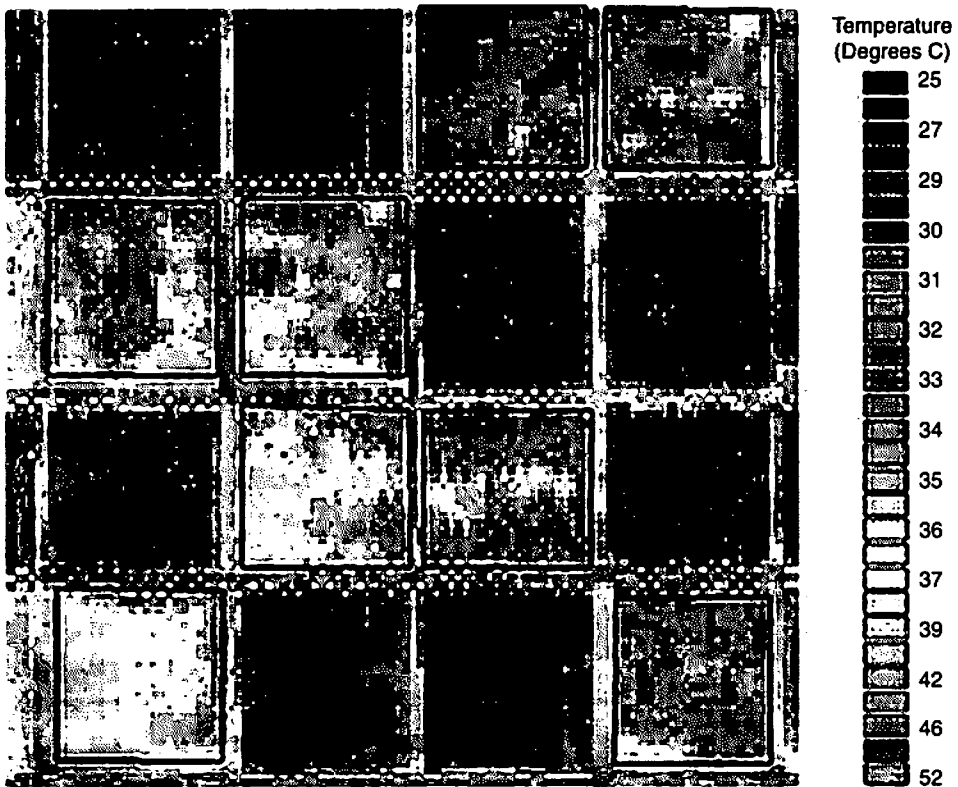


Figure 12.3 Surface temperature image acquired on July 28, 1999 between 12:30 and 14:30 MST over a cotton field near Phoenix, Arizona, with differential water treatments derived from a scanning infrared thermometer mounted on a linear move irrigation system. See Barnes et al. (2000) for additional experimental details and see CD-ROM for color image.

crop water stress. In this section we link the stress-induced physiological and anatomical changes in plant leaves and canopies to spectral responses in the visible, NIR, SWIR, and SAR wavelengths.

Turner (1977) provided a good synthesis of the effects of water deficit on crop plants and the physiological adaptations to transient stress. He identified crop physiological adaptations associated with three types of drought resistance, where *drought* was defined as a period without significant rainfall (Table 12.2). These physiological adaptations ranged from changes in canopy architecture to adjustments in leaf osmotic potential. The following discussion is focused on the physiological adaptations that might have the greatest effect on spectral reflectance and SAR backscatter and the optical properties of plants that would allow stress detection with remote sensing.

Drought escape is the ability of the plant to complete its life cycle before serious soil and plant water deficits develop. For example, studies have shown that wheat can hasten maturity in response to mild water deficits at the critical time between flowering and maturity (Turner, 1977). Alternatively, when stress occurred between floral initiation and wheat ear emergence, the number of wheat tillers that produced ears was less than under well-watered conditions (Turner, 1977). These are examples of the rapid phenological development and developmental plasticity that have been associated with water stress conditions at critical crop phenologic stages.

Drought tolerance at high tissue water potential is sometimes referred to as *drought avoidance* since it allows plants to endure drought periods while maintaining a high plant water status. One such crop adaptation is the reduction of water loss through increased stomatal and cuticular resistance. This is expressed in increased epidermal waxes of leaves and a reduction in general plant productivity. Another adaptation is to reduce the radiation absorbed by the plant through leaf movement (e.g., leaf cupping, paraheliotropism, or wilting) or increased leaf pubescence and waxiness. Drought tolerance is also achieved by reduction of leaf area through de-

TABLE 12.2 Mechanisms of Drought Resistance

Drought escape
Rapid phenological development
Developmental plasticity
Drought tolerance at high water potential
Reduction in water loss
Increase in stomatal and cuticular resistance
Reduction in radiation absorbed
Reduction in leaf area
Maintenance of water uptake
Increased root density and depth
Drought tolerance at low water potential
Maintenance of turgor
Osmotic adjustment
Increase in elasticity
Decrease in cell size
Desiccation tolerance
Protoplasmic tolerance

Source: Adapted from Turner (1977).

creased leaf expansion, reduced tillering and branching, and leaf shedding. Some crops maintain a high plant water status by increased root growth, resulting in decreased top growth and less investment in photosynthetic surface.

Water stress is often expressed by the inability of some crop species to maintain cell turgor at low water potentials. The elasticity of crops to control cell turgor varies widely by species. For example, in a field study with maize, sorghum, and tobacco, Turner (1977) found that sorghum had a lower soil water potential than tobacco at zero turgor. He also reported that although tobacco and maize had equivalent turgors at high leaf water potentials, maize had a lower water potential than tobacco at zero turgor. These variations in cell turgor under drought conditions can influence the closure of stomatal apertures, and the rates of photosynthesis, evaporation, and leaf expansion.

12.2.3 Optical Properties of Plant Leaves

There has been a great deal written on the optical properties of crop leaves in the visible, NIR, TIR, and SWIR domains (e.g., Bauer, 1985). In the visible domain, leaf reflectance is affected primarily by leaf pigments such as chlorophyll, xanthophyll, carotenoids, and anthocyanins. Thomas and Oerther (1972) found that with nitrogen deficiency, the visible reflectance increased (due to decreasing chlorophyll content) and the NIR and SWIR reflectances decreased (due to decreasing number of cell layers). In the NIR, reflectance depends on the anatomical structure of the leaves and increases with the number of cell layers and the size of the cells. In the TIR, there is a direct link between the process of plant water evaporation and the plant thermal response (i.e., water evaporates and cools the leaves). In the SWIR, the reflectance is mainly affected by the leaf water content, with strong water absorption bands at 1.45, 1.95, and 2.7 μm . It is generally reported that leaves under stress show a decrease in reflectance in the NIR spectrum, a reduced red absorption in the chlorophyll active band (0.68 μm), and a consequent blue shift of the red-edge. However, Guyot et al. (1984) found that it was necessary to have an extremely severe water stress to affect the leaf reflective properties.

Some of the leaf physiological adaptations to stress discussed in previous sections have an effect on leaf reflectance. For example, increasing leaf pubescence results in an increased reflectance in the visible and SWIR spectral bands, but has little effect on NIR reflectance. Gausman (1983) explained that since such hairs are made of cellulose and are dry, they appear white in the visible spectrum, transparent in the NIR, and highly reflective in the SWIR, except for absorptions in cellulose bands. Also, increases in leaf waxiness affect the specular component of leaf reflectance and can increase leaf reflectance substantially, depending on the incidence angle of the incoming radiation.

The optical properties of leaves in the radar spectrum covered by orbiting sensors are defined by the domination of the dielectric constant of water. The relative dielectric constant of water (and healthy leaves) is about 80 and the dielectric constant of dry vegetation and soil is on the order of 2 to 3 (Ulaby et al., 1984). Based on this information, electromagnetic modeling approaches have successfully described the SAR scattering that would result from the simple shapes that make up a crop canopy.

12.2.4 Optical Properties of Plant Canopies

Although knowledge of the optical properties of individual leaves contributes to our understanding of the processes involved, field studies have shown that spectrophotometer studies of single leaves can be very misleading for predicting reflectance from crops. For example, Guyot et al. (1984) reported that the most important factor that influences the reflectance of a plant canopy is its geometrical structure, not its leaf reflectance. He stated that the reflectance in visible and NIR wavelengths is determined primarily by the green leaf area index (GLAI) and the average leaf inclination angle. Effects of variations in leaf inclination distribution function (LIDF) increased with GLAI and were greater in red-NIR subspace than in red-green subspace. Jackson and Ezra (1985) concluded that stress-induced changes in visible, NIR, and SWIR reflectance of a cotton canopy were due largely to canopy geometry changes rather than leaf physiological/anatomical changes in all but the red spectral band. Furthermore, Myers et al. (1983) identified seven parameters (in addition to leaf reflectance) that determined crop canopy reflectance, of which only the first three could be related directly to crop stress: (1) transmittance of leaves, (2) amount and arrangement of leaves, (3) characteristics of other components of the vegetation canopy, (4) characteristics of the background, (5) solar zenith angle, (6) look angle, and (7) azimuth angle.

Similarly, the TIR emittance of a plant canopy is a function of the temperatures of both the plant components and the soil. T_c , the canopy temperature, is defined by Norman et al. (1995) as the TIR temperature in which the "vegetation dominates the [measurement] field of view minimizing the effect of soil." T_0 is the temperature of the soil surface. T_s is the surface composite temperature, defined by Norman et al. (1995) as the "aggregate temperature of all objects comprising the surface," which was shown by Kustas et al. (1990) to be a function of T_c and T_0 , where

$$T_s^4 = f_c T_c^4 + (1 - f_c) T_0^4 \quad (12.4)$$

and f_c represents the fractional cover of the vegetation and all temperatures are in kelvin. When the surface is covered completely by vegetation, $T_s = T_c$, and when the surface is bare soil, $T_s = T_0$.

As with the optical spectrum, SAR scattering within the crop canopy is a complex function of the relative positions and spatial densities of the plant constituents and such soil properties as roughness and moisture. Furthermore, SAR backscatter is a function of the wavelength, polarization, and incidence angle of the illumination source. Nonetheless, there is empirical and theoretical evidence that SAR backscatter may provide useful information about crop water stress (Moran et al., 1997c; 1998). At high frequencies (about 13 GHz), field experiments have shown that the radar signal was particularly sensitive to such plant parameters as GLAI, plant biomass, and percentage of vegetation cover. At low frequencies (about 5 GHz), many studies have shown that the radar signal was very sensitive to soil moisture, although this sensitivity decreased with increasing vegetation cover.

12.3 REMOTELY SENSED INFORMATION FOR MANAGEMENT OF IRRIGATED AGRICULTURE

The Ag20/20 consortium of members of corn, cotton, soybean, and wheat commodity groups identified their highest-priority information needs for agricultural management (Table 12.1). In the following sections, the potential applications of remote sensing and the actual remote sensing products related to each information need are summarized. Although many examples are presented, the type and magnitude of the remotely sensed manifestation of crop physiological status presumably will vary with the type of crop and the attendant cultural practices. Thus, factors such as whether the crop is an annual or a perennial, a row crop or a woody crop, whether it displays small or large row spacing, as well as various other factors may all affect the application and calibration of remotely sensed estimates of a crop's physiological status.

12.3.1 Irrigation and Water Information

Over the past 30 years, remotely sensed data have been used successfully for deriving information useful for irrigation scheduling and management. The basic approaches have focused on parameters related directly to crop water status [e.g., crop water loss (evaporation), metabolism, conductance, and photosynthesis] and plant manifestations of chronic crop water stress (e.g., phenologic stage and leaf expansion and loss).

12.3.1.1 CROP EVAPORATION

An important breakthrough in the use of remote sensing for irrigation management was development of the Idso-Jackson crop water stress index (CWSI) (Idso et al., 1981; Jackson et al., 1981). Jackson et al. (1981) derived the theoretical CWSI (CWSI_t) based largely on equation (12.3). Taking the ratio of actual (E for any r_c) to potential (E_p for $r_c = r_{cp}$) crop evaporation rate gives

$$\frac{E}{E_p} = \frac{[\Delta + \gamma^*]}{[\Delta + \gamma(1 + r_c/r_a)]} \quad (12.5)$$

where $\gamma^* = 1 + r_{cp}/r_a$ (RPA/°C), with r_{cp} being the canopy resistance at potential evaporation. Jackson et al. (1981) defined the CWSI_t, ranging from 0 (ample water) to 1 (maximum stress), as

$$\text{CWSI}_t = 1 - \frac{E}{E_p} = \frac{\gamma(1 + r_c/r_a) - \gamma^*}{\Delta + \gamma(1 + r_c/r_a)} \quad (12.6)$$

To solve equation 12.6, a value of r_c/r_a is obtained by rearranging equation 12.3 and assuming that G is negligible for a full-cover canopy, where

$$\frac{r_c}{r_a} = \frac{[\gamma r_a R_n / \rho C_p] - [(T_c - T_a)(\Delta + \gamma)] - \text{VPD}}{\gamma[(T_c - T_a) - r_a R_n / \rho C_p]} \quad (12.7)$$

and r_c/r_a is substituted into equation 12.6 to obtain the CWSI.

Although Jackson et al. (1981) provided a thorough theoretical approach for computation of CWSI, the concept is more universally applied using a semiempirical variation proposed by Idso et al. (1981) based on the *non-water-stressed baseline*. This baseline is defined by the relation between $(T_c - T_a)$ and VPD under nonlimiting soil moisture conditions (i.e., when the plant water is evaporating at the potential rate) (Figure 12.2). Such non-water-stressed baselines have been determined for many different crops, including aquatic crops and grain crops for both preheading and postheading growth rates (Idso, 1982). The commercial applicability of CWSI is evidenced by the commercial production of a handheld instrument designed to measure CWSI, several commercial imaging companies that are providing CWSI to farmers, and the multitude of examples of application of this theory with airborne and satellite-based thermal sensors combined with ground-based meteorological information (see reviews by Moran and Jackson, 1991; Norman et al., 1995).

Application of CWSI with satellite- or aircraft-based measurements of surface temperature is generally restricted to full-canopy conditions, so that the surface temperature sensed is equal to the canopy temperature. To deal with partial plant cover conditions, Moran et al. (1994) developed a water deficit index (WDI), which combined measurements of reflectance with surface temperature measurements (a composite of both the soil and plant temperatures), as expressed by

$$\text{WDI} = 1 - \frac{E}{E_p} = \frac{(T_s - T_a)_m - (T_s - T_a)_r}{(T_s - T_a)_m - (T_s - T_a)_x} \quad (12.8)$$

The WDI is operationally equivalent to the CWSI for full-cover canopies, where measurement of $T_s = T_c$. Graphically, WDI is equal to the ratio of distances AC/AB in the trapezoidal shape presented in Figure 12.4, where $\text{WDI} = 0.0$ for well-watered conditions and $\text{WDI} = 1.0$ for maximum stress conditions. That is, the left edge of the vegetation index-temperature (VIT) trapezoid corresponds to $(T_s - T_a)$ values for surfaces evaporating at the potential rate; the right edge corresponds to $(T_s - T_a)$ values for surfaces in which no evaporation is occurring. In practice, WDI utilizes the Penman-Monteith energy balance equation to define the four vertexes of the VIT trapezoid, which encompasses all possible combinations of a spectral vegetation index [e.g., soil adjusted vegetation index (SAVI)] and $(T_s - T_a)$ for one crop type on one day (Figure 12.4).

Another promising approach for operational application is the use of remotely sensed crop coefficients (the ratio of actual crop evaporation to that of a reference crop) for estimating actual site-specific crop evaporation rates from readily available meteorological information (e.g., Bausch, 1993). This approach requires only a measure of NDVI and is simply an improvement of an approach already accepted and in use by farmers to manage crops, where such improvements include increases in accuracy of the evaporation estimates and, with the use of images, the ability to map within- and between-field variations.

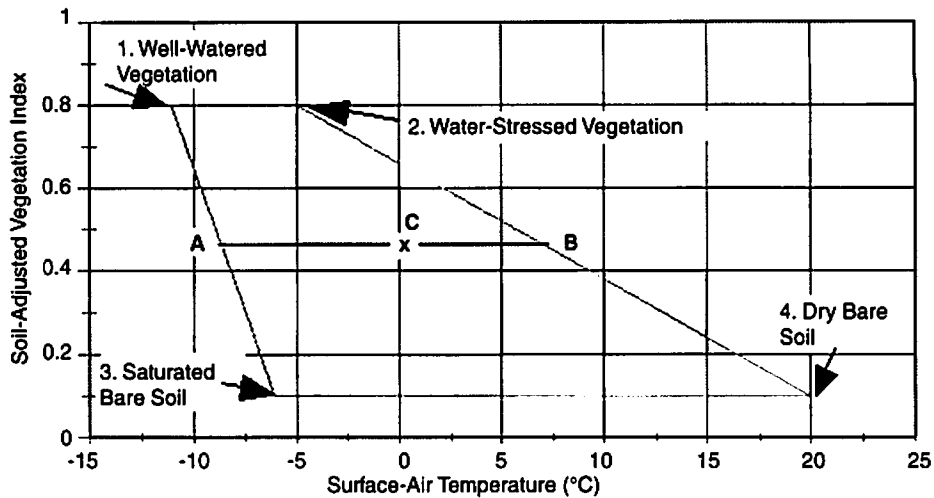


Figure 12.4 Trapezoidal shape that would result from the relation between surface temperature minus air temperature ($T_s - T_a$) and the soil-adjusted vegetation index (SAVI). With a measurement of $T_s - T_a$ at point C, the ratio of actual to potential evaporation is equal to a ratio of the distances CB and AB. (Data from Moran et al., 1994.)

12.3.1.2 CROP METABOLISM

Quite distinct from the CWSI and WDI, Burke et al. (1988) developed a concept of thermal stress in plants that linked the biochemical characteristics of a plant with its optimal leaf temperature range. The *thermal kinetic window* (TKW) is the range of temperatures within which the plant maintains optimal metabolism. For example, the TKW for cotton growth is 23.5 to 32°C, with an optimum temperature of 28°C, and biomass production is related directly to the amount of time that canopy temperatures are within the TKW (Figure 12.5), provided that insolation, soil moisture, and nutrients are nonlimiting. The TKWs have been identified for several crop and forage species (Table 12.3).

In practice, the TKW provides a biological indicator of plant health that could potentially be used for irrigation management. In a patent application (SN 261510, filed June 17, 1994), the inventors (Upchurch, Wanjura, Burke and Mahan) describe an irrigation method in which the canopy temperature (T_c) of a target plant is measured repeatedly with an infrared thermometer at a regular time interval (t_i), and T_c is compared with the optimum plant temperature (T_{c_o}). If $T_c \leq T_{c_o}$ or if the VPD is restrictive to plant cooling, irrigation is not indicated. If both $T_c > T_{c_o}$ and VPD are not restrictive to plant cooling, t_i is added to a time register. When the accumulated time in the time register exceeds the time threshold, evaporative cooling to reach the optimum is feasible, and a signal to the irrigation unit is generated.

12.3.1.3 CROP CONDUCTANCE AND CANOPY WATER CONTENT

The CWSI, WDI, and TKW are good examples of indexes linking surface temperature measurements to crop and soil evaporation rates. There have been far fewer studies that link surface reflectance directly to SD. Jackson et al. (1983) reported

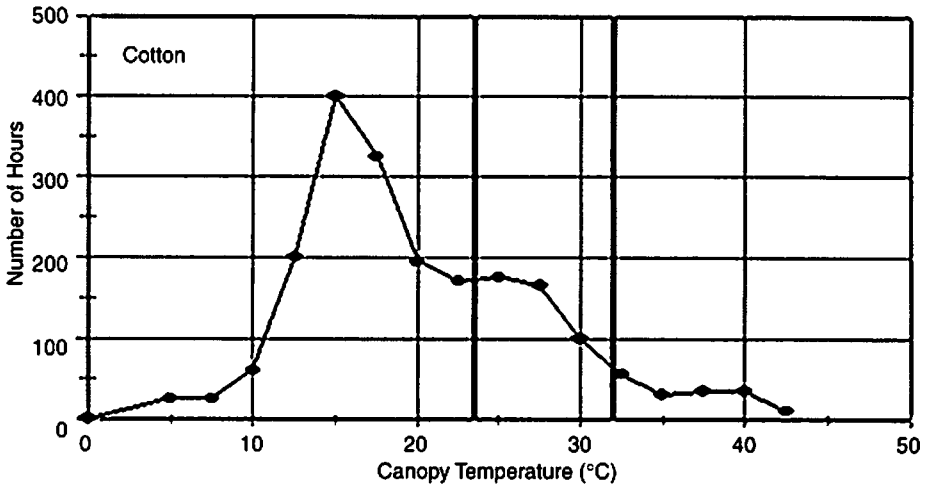


Figure 12.5 Seasonal canopy temperatures of cotton, where the vertical lines represent the temperature range that comprises the species-specific thermal kinetic window (TKW) as determined from the changes in the apparent K_m with temperature. (Data from Burke et al., 1988.)

that season-long measurements of reflected solar radiation will not detect the onset of stress and are sensitive to stress only after plant growth has been retarded. Jackson and Pinter (1986) explained that plant temperatures indicate the degree of stress at a particular time, whereas reflectance measurements integrate the effects of stress over time.

Sellers et al. (1992) proposed a theoretical foundation for a relation between the spectral vegetation index and the relative response of unstressed canopy conductance (g_c^*) to changes in incident PAR flux (F_0), where $\nabla_F = \partial g_c^* / \partial F_0$. They reported a near-linear relation between ∇_F and the ratio of NIR/red reflectance on a site-by-site basis. This relation has potential for use in calculating field-scale potential evaporation rates from surface reflectance measurements, but will not be useful for discriminating crop stress conditions.

There are few studies linking canopy reflectance with the percent water content of total canopy biomass, despite the strong relations reported between leaf spectral

TABLE 12.3 Summary of Thermal Kinetic Windows and Optimum Canopy Temperatures for a Variety of Crops and Garden Plants

Crop	T_c (°C) Range	Optimum
Cotton	23.5–32.0	27.5
Wheat	17.5–23.0	20.0
Cucumber	23.5–39.0	35.0
Bell pepper	23.0–41.0	32.0
Tomato	20.5–24.5	22.5
Petunia	18.0–28.0	25.0
Potato	15.0–25.0	20.0
Soybean	15.0–30.0	25.0

reflectance (particularly in the SWIR spectrum) and leaf water content (Ripple, 1986; Cohen, 1991a,b). The published literature is somewhat confusing on this point since some studies correlate canopy spectral reflectance with total plant water content (g/m^2), and others report relations with percent water content and water content per unit leaf area (g/m^2). The total plant water content is primarily a function of plant biomass (Gardner et al., 1985), whereas the percent water content and water content per unit leaf area are related to plant hydric conditions (Guyot et al., 1984; Fourty and Baret, 1997). In any case, poor results have been obtained in studies correlating surface reflectance measured in wide spectral bands with percent water content and water content per unit leaf area. Both Bowman (1989) and Hunt and Rock (1989) concluded that the small change in leaf water content associated with a relatively large change in turgor pressure, stomatal conductance, and photosynthesis required very accurate measurements of reflectance to estimate canopy water status adequately. Hunt and Rock (1989) stated emphatically that for most plants "indexes derived from NIR and [SWIR] reflectances cannot be used to remotely sense water stress." Other studies were less conclusive. For example, Guyot et al. (1984) reported a moderate correlation between wheat canopy reflectance in the SWIR domain and the percent water content of the main shoot. However, they found that the SWIR reflectance was also affected by seasonal variations in percent vegetation cover, and in some cases, this played the main role in determining SWIR reflectance.

12.3.1.4 CROP PHOTOSYNTHESIS

Measurements of leaf chlorosis, which cause diminished leaf photosynthetic capacity, may be particularly suitable for early water stress detection. A spectral index that has been closely related to leaf chlorophyll concentration is the *red-edge*, where the red edge is the position of maximum rate of change along the vegetation reflectance spectrum (in units of wavelength). The red-edge occurs between the wavelengths of 0.69 and 0.76 μm due to the change in reflectance caused by chlorophyll absorption in the red spectrum and multiple scattering from leaves in the NIR spectrum (Filella and Peñuelas, 1994) (Figure 12.6). Although the red-edge may be a good estimator of leaf chlorophyll levels, there is some controversy about its utility at canopy levels (Demetriades-Shah et al., 1990).

Studies of the red-edge have necessarily required measurements of canopy reflectance using high-spectral-resolution (1 to 10 nm) field spectroradiometers covering the visible and NIR spectrum. Although the use of hyperspectral remote sensing diverges from this chapter's focus on broad spectral bands, such studies of high-spectral-resolution reflectance have been useful for defining the best broad spectral bands (20 to 100 nm) used to discriminate water stress conditions. In a simulation study of spectral bands that could be most useful for monitoring several crop canopy characteristics, Fourty and Baret (1997) suggested that 20 nm wavelength bands could retain the hyperspectral information associated with percent plant water content and still allow adequate signal-to-noise ratio for satellite-based sensors.

For determination of crop water stress, several studies have proposed ratios of two complementary narrow-wavelength bands where the reflectance in one wavelength was sensitive to water or chlorophyll concentrations, and the reflectance of another (a "reference") was relatively insensitive to such concentrations. Peñuelas

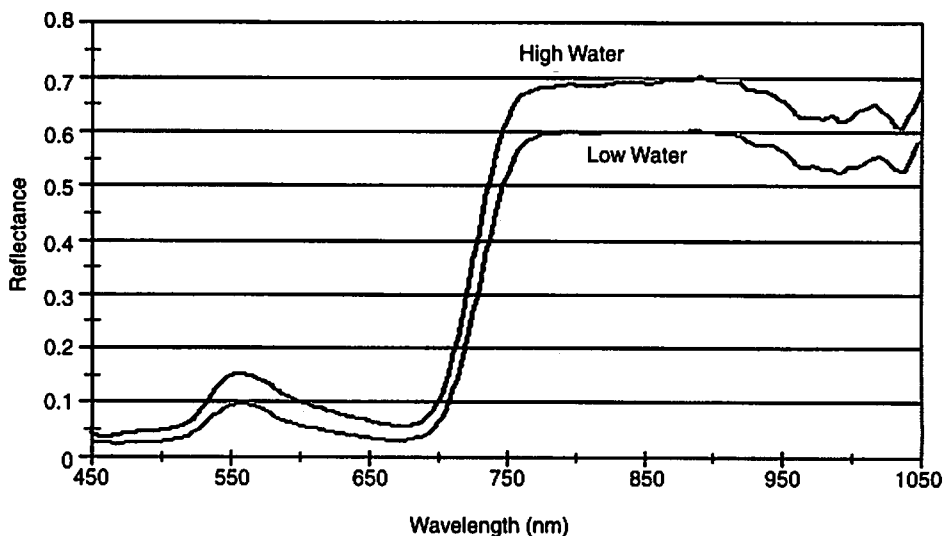


Figure 12.6 Expected trends of spectral reflectance of a crop canopy with high- and low-water treatments. (Data from Filella and Peñuelas, 1994.)

et al. (1997) developed a water index (WI), defined as the ratio between reflectances at 0.97 and 0.90 μm for measurement of the percent plant water content for drought assessment. Gao (1996) introduced the normalized difference water index (NDWI), defined as the difference between reflectances at 0.86 and 1.24 μm divided by their sum. In a qualitative demonstration, the NDWI appeared to be sensitive to the liquid water content of vegetation canopies. Carter and Miller (1994) showed that the ratio of reflectances at 0.694 and 0.760 μm could be used to detect stress simultaneously with the crop physiological manifestation. Such indexes, based on narrow spectral bands, may have limited success with aircraft- and satellite-based sensors because they may be affected by *atmospheric* water absorption as well as plant water absorption.

All three of the above-mentioned spectral indices were found to be sensitive to measurements of plant stress as well as variations in ground coverage by leaves. To minimize the effects of ground cover variations and to maximize the assessment of plant stress condition, both Gao (1996) and Peñuelas et al. (1997) suggest that the WI and NDWI be further normalized using a ratio or multiple regression with a vegetation index (e.g., NDVI) to correct for changing vegetation cover. This multispectral approach could circumvent the complexity associated with hyperspectral sensors by allowing a sensor to be designed with only a few spectral bands at strategic narrow and broad wavelength bands (assuming that wavelength and radiance calibrations are reliable). On the other hand, these indexes have been tested only for selected crops and they may be crop specific.

12.3.1.5 CROP PHENOLOGIC STAGE

There is evidence that crop water stress can either hasten (Turner, 1977) or delay (Idso et al., 1980) crop development, depending on the crop phenologic stage at

the time of water stress. Also, the time and duration of stress are of critical importance to ultimate yield (e.g., if a period of water stress occurs during heading or during the grain-filling period, the reduction of the grain yield is much greater than if this same stress condition occurs at some other time). For these reasons, knowledge of phenologic stage relative to planting date could provide important information on crop stress.

Multiple observations of the temporal-spectral characteristics of crops offer promise for use in estimating the crop development stages at the time of interest. Several approaches have been proposed to provide a spectral crop calendar. Tucker et al. (1979) showed that crop phenologic stage could be determined using a combination of spectral data and accumulated temperature units (growing degree-day). Badhwar and Henderson (1981) suggested that a given crop has a unique spectral profile in time and that the fractional area under the greenness profile curve was closely related to development stages in corn and soybeans. Malila et al. (1980) used the temporal changes in red and NIR reflectance of a wheat canopy related to crop development to develop a correlation between crop phenologic stage and canopy reflectance. That is, during the initial growth stage, NIR reflectance increased and red reflectance decreased due to corresponding differences in soil and green leaf reflectances. At heading, heads apparently cast shadows, causing both the NIR and red reflectance to decrease; and during ripening, the combined reflectance of the heads, the senescing leaves, and the exposed soil caused the red reflectance to increase while the NIR reflectance continued to decline.

There have also been attempts to determine stress effects by monitoring the temporal duration of specific phenologic stages. For example, Idso et al. (1980) reported that for wheat plots stressed for water, senescence appeared to be drawn out over a longer period of time than for well-watered plots. This was apparently due to an evolutionary strategy for annual plants to prolong their life span to increase grain production under stressful conditions. Idso et al. (1980) related the slope of the vegetation index (VI) over time to the rate of senescence and correlated this slope with final grain yield for wheat and barley under stressed and nonstressed conditions (Figure 12.7). In a similar study, Fernández et al. (1994) found that the hydric stress of wheat could be determined by the slope of the NDVI along the maturity stage.

12.3.1.6 LEAF EXPANSION AND LOSS

Crop water stress can also manifest itself in reduced leaf expansion and leaf loss. In such cases, measurements of crop biomass and GLAI can provide information on the degree, duration and spatial extent of crop stress. Numerous studies have reported a strong correlation between red and NIR canopy reflectances and GLAI or crop biomass (e.g., Tucker, et al. 1979). The spectral data used in such correlations often take the form of a vegetation index, which is a ratioed or linear combination of reflectances (ρ) in two or more spectral bands, generally the red (ρ_{red}) and NIR (ρ_{NIR}). The most commonly used vegetation indexes are the simple ratio ($SR = \rho_{red}/\rho_{NIR}$) and the normalized difference vegetation index [$NDVI = (\rho_{NIR} - \rho_{red})/(\rho_{NIR} + \rho_{red})$].

Several studies have monitored stress-induced reductions in biomass and GLAI using remote sensing techniques. Fernández et al. (1994) reported that water stress had a greater effect than lack of fertilizer on leaf area of wheat plants. Water-stressed

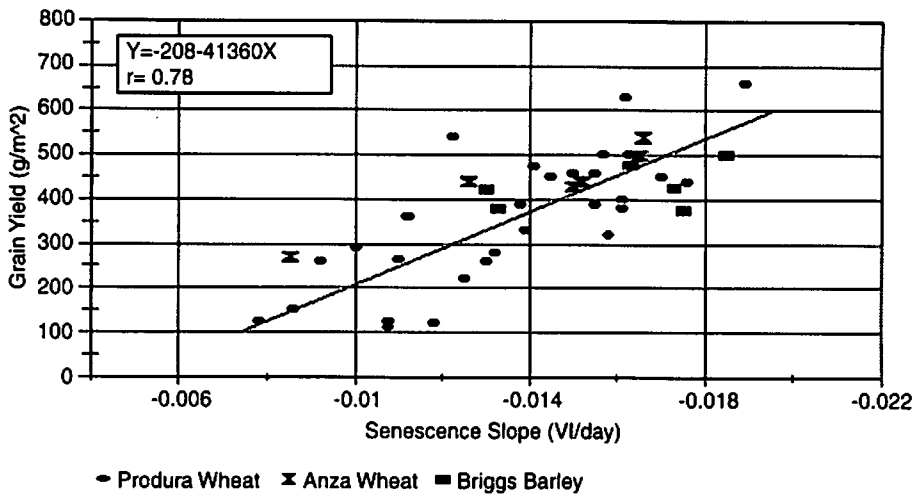


Figure 12.7 Final grain yield of Produra wheat, Anza wheat, and Briggs barley versus the slope of the transformed vegetation index (TVI6) during the senescence period. (Data from Idso et al., 1980.)

plants were 20 to 30% shorter than nonstressed plants and had 22 to 27% less dry biomass. They found a strong correlation between the stress-induced differences in GLAI and the NDVI, with a reported coefficient of variation of 0.15 between measured and estimated GLAI. Gardner and Blad (1986) studied the effects of moisture stress on the reflectance of corn and found that reductions in GLAI accounted for nearly all of the variation in spectral response. Furthermore, when these varying levels of spectral response were accumulated over time, the sum was strongly related to grain yield (Walburg et al., 1982).

Mogensen et al. (1996) reported that relative leaf expansion rate was a more sensitive expression of water stress than SD and could be used for early detection of crop water stress. Their study had two interesting conclusions related to the detection of crop water stress for a rape crop. They found that stress early in the season had more influence on dry plant matter accumulation than did late-season drought of similar intensity and duration. Further, they were able to monitor crop stress throughout the season using a relative reflectance index (RRI; the ratio between the reflectance of the water-stressed and fully irrigated crop).

Although these results are encouraging, this approach is limited by the fact that the reflectance–GLAI relation is exponential, leading to a saturation of the NIR response at GLAI values of 5 to 6 (Bauer, 1985). A better measure of effects of water stress on leaf expansion and biomass production might be the amount of solar radiation intercepted, which is related directly to plant growth. Kumar and Monteith (1981) showed that the fraction of absorbed photosynthetically active radiation (fAPAR) was related linearly with NIR/red reflectance and could be used to estimate the dry matter of sugar beets. More recent work by Pinter (1993) has shown that this relation between the spectral vegetation index and fAPAR was independent of variations in solar zenith angle, thus increasing the usefulness of this remote sensing approach.

12.3.2 Nutrient Application

Like crop water stress, crop nutrient stress has a direct effect on crop growth, development, yield, and ultimately on growers' profits. Growers face competing goals when managing fertilizer application. Nitrogen is frequently the major limiting nutrient in agricultural soils, and growers must supply enough nitrogen to their crops while minimizing the loss of nitrogen to the environment. Nitrogen lost to the environment not only represents an economic loss to the grower but has been shown to be a serious threat to water quality. Yet the economic penalties associated with reduced yields from supplying inadequate nitrogen to crops are substantial. Achieving this balance may be further complicated for those nutrients, such as nitrogen, that are water soluble and highly mobile in the soil profile, especially if the crop is irrigated. Growers need an operational means to quantify plant nutrient stress and to evaluate the effects of stress on the crop at each stage in its development. In the following sections we present the plant manifestations of nutrient stress that can be detected with measurements in the visible and near-infrared wavelengths. The discussion centers almost exclusively on the optical manifestations of leaf and crop nitrogen deficiencies, a choice motivated by the level of understanding of the optical manifestations of nitrogen deficiencies as compared to those of other nutrient deficiencies.

12.3.2.1 OPTICAL MANIFESTATIONS OF CROP NUTRIENT VARIABILITY

Leaves deficient in nitrogen absorb less and scatter more visible light, a research result both well established and understandable given the importance of nitrogen in photosynthesis biochemistry (e.g., Schepers et al., 1996). At low to moderate concentrations, leaf nitrogen is found mostly in chlorophyll molecules, the primary light absorbing molecule in the leaf (Yoder and Pettigrew-Crosby, 1995; Daughtry et al., 2000). At high nitrogen levels, the relationship between leaf chlorophyll and leaf nitrogen concentrations may be nonlinear, indicating the presence of nonchlorophyll nitrogen, probably $\text{NO}_3\text{-N}$ (Daughtry et al., 2000). Thus, the concentration of viable chlorophyll molecules decreases in tandem with decreases in the concentration of leaf nitrogen, and as a consequence, the leaf absorption of PAR decreases and scattering increases. Measurements of the light-scattering properties of a leaf provide an indirect indicator of the leaf chlorophyll content, which in turn provides an indirect indicator of the leaf nitrogen content. Visually, leaves marginally deficient in nitrogen may appear a lighter, less saturated shade of green. More severely nitrogen-stressed leaves may appear yellowish green and chlorotic. For deficiencies of many nutrients other than nitrogen, leaf optical properties, although less well researched, are generally similar to those of nitrogen-deficient leaves. Leaves deficient in these other nutrients tend to absorb incident PAR light less efficiently and scatter more PAR light. (By definition, scattering + absorption equals 1.0; scattering equals hemispherical reflectance + hemispherical transmittance. For leaves, spectral curves representing hemispherical reflectance and hemispherical transmittance generally appear closely similar and are sometimes assumed equal.)

Thus, individual leaves deficient in N, P, K, S, Ca, Mg, Mn, Fe, Zn, and possibly As, Co, and Ni, generally display increased hemispherical reflectance, increased hem-

ispherical transmittance, and decreased absorptance in the photosynthetically important visible wavelength region (Al-Abbas et al., 1974; Walburg et al., 1982; Milton et al., 1989, 1991; Adams et al., 1993; Mariotti et al., 1996; Masoni et al., 1996). In fact, leaf optical responses to deficits of these nutrients are generally sufficiently similar in the PAR region that efforts have been unsuccessful to invert leaf spectral reflectance and transmittance to both identify the nutrient deficiency and estimate its magnitude. On the other hand, if the deficiency involves the leaves of only one plant species and only one nutrient, both known *a priori*, the magnitude of the deficiency may be estimated from such optical measurements (Masoni et al., 1996). Although the optical manifestations of nutrient deficits in leaves are understood in general, much research remains to be conducted, especially on the effects of nonnitrogen nutrients.

Spectra of chlorophyll, measured *in vitro*, show light absorption to be concentrated in two narrow bands around 0.44 and 0.68 μm in the blue and red wavelength regions, with lesser amounts of light absorbed at wavelengths between these two bands. Green leaf spectra, which are dominated by light absorption due to chlorophyll, display similar light absorption features, although the absorption bands are characteristically wider in wavelength (Merzlyak et al., 1999). While the primary optical manifestation of many leaf nutrient deficits is generally an increase in the leaf reflectance in the visible region, the reflectance changes generally do not occur equally at all wavelengths in the visible. Instead, these leaf reflectance changes occur in concert with the optical properties of chlorophyll. As two endpoint cases, consider leaves severely deficient in nitrogen and leaves having adequate or excessive nitrogen. In the first case, when leaf nitrogen, and therefore chlorophyll, concentrations begin to increase from near zero, the depth of the absorption well at 0.68 μm increases accordingly, asymptotically approaching 100% absorption of the light that enters the leaf. (Note that not all of the light incident on the leaf subsequently enters the leaf; a small amount, generally between 2 and 5%, is reflected by the leaf surface.) In the second case when leaf nitrogen is adequate, most light entering the leaf is absorbed at a wavelength of 0.68 μm , and leaf reflectance and transmittance display minimal decreases as leaf nitrogen increases. In fact, Gitelson and Merzlyak (1997, 1998) found leaf reflectance at 0.67 μm is virtually insensitive to chlorophyll variation. However, at adjacent wavelengths on the two shoulders of the 0.68- μm absorption well, increases in leaf nitrogen do manifest increases in the light absorbed. (The resulting movement of the red-edge is described below.) Of particular interest are the green wavelength region around 0.55 μm and the NIR region near 0.71 μm (Gitelson and Merzlyak, 1997). As leaf nitrogen concentration increases from near zero to adequacy, there is a corresponding increase in leaf absorption around 0.55 μm and near 0.71 μm and a corresponding decrease in both leaf reflectance and transmittance. This reveals the diagnostic potential of optical measurements in both wavelength regions over an extremely large range of leaf nitrogen concentrations (Gitelson and Merzlyak, 1997). Protocols for estimating leaf nitrogen concentrations often involve measurements at these two wavelengths.

Nutrient deficits in crop canopies have the potential to affect canopy architecture in addition to the optical properties of not only the leaf but also the stem and flower/grain head. Canopy architecture and the optical properties of canopy components are two of the three factors that determine canopy reflectance. Many characteristics of canopy architecture (e.g., canopy height, plants per unit area, leaf area index,

aboveground biomass, and the size and location of both the inflorescence and the canopy grain head) depend on the time integration of the photosynthesis process. If canopy growth is limited by light but not by water or nutrients, the time integral of the photosynthetically active radiation absorbed by foliage in the canopy determines the amount of photosynthetic product produced (Monteith, 1977). This, in turn, affects canopy architectural properties and canopy reflectance. If the canopy is both nutrient and light limited, lack of key nutrients will tend to decrease, the amount of PAR absorbed by the leaves (discussed above). The amount of photosynthetic product produced by the leaves will tend to decrease and in response, the canopy as it grows will tend to modify its architecture to accommodate the decreased availability of photosynthetic products. Manifestations of typical nutrient stresses generally appear initially as changes in the optical properties of leaves and only later as changes in the canopy architecture. Thus, the direction and magnitude of these changes in canopy spectral reflectance depend directly on the duration and severity of the disruption of the leaves' photosynthesizing apparatus, as well as the crop development stage when the disruption begins.

Decreased canopy biomass is probably the most common architectural manifestation of chronic canopy nutrient stress, provided that the stress occurs during vegetative growth stages prior to the maximum vegetative stage. Jensen (1990) and Serrano et al. (2000) point out that under nonlimiting water supply, the nitrogen status of a crop is the major factor controlling the rate of biomass accumulation. Thus, the radiance of a nutrient-stressed canopy in the vegetative growth phase tends to be greater (slight increase in the red, more in the green) in the visible spectral region and less in the NIR region. Examples of this can be seen in the reflectance of canopies of corn reported by Walberg et al. (1982) and wheat reported by Filella et al. (1995).

The consequences of the onset of nutrient stress during the crop reproductive growth stages tend to be less universal and usually less evident. The reflectance of nutrient-stressed leaves, just as during vegetative growth, tends to increase and may affect canopy reflectance. The amount of grain produced tends to decrease, but that effect does not generally manifest changes in the canopy reflectance. Nutrient stress may also affect the canopy architecture, as in the case of sunflower, and canopy reflectance. Nutrient deficits during canopy vegetative growth manifest two primary effects: an increase in the PAR light scattered by leaves and stems, and a decrease in canopy biomass. Both effects are usually evident in canopy spectra; however, the effects of crop nutrient deficits during the reproductive phase are more varied and crop specific and may not be as evident in canopy spectra.

Canopy architecture and the directions of illumination and observation serve to modulate the light-scattering properties of the canopy components (i.e., leaves, stems, flower/grain head, and soil). Canopy architecture does not introduce into the canopy spectra any spectral features that do not already exist in the spectra of the canopy components. A feature in the spectra of the leaves in a canopy layer may not be evident in canopy spectra if the leaves are not observable and/or are not illuminated because the leaf layer is located at the bottom of the canopy architectural structure. For example, severely nitrogen-deficient romaine lettuce translocates nitrogen from the older outer leaves into the expanding leaves in the whorl, which is often partially obscured by adjacent older foliage. Because of this obfuscation, estimates based on canopy radiance measurements presumably would underestimate

canopy nitrogen concentrations. As another example, perhaps the only commonly observed narrowband absorption in soils is due to iron and is located at approximately $0.9 \mu\text{m}$. Presumably, this absorption feature would more probably be evident in spectra of a canopy having a low rather than a high biomass.

12.3.2.2 RED-EDGE POSITION FOR DETERMINING CROP NUTRIENT STRESS

The position of the red-edge (an abrupt, almost step increase in the leaf reflectance in the NIR around $0.72 \mu\text{m}$ just outside the visible region) offers a robust metric for monitoring leaf and canopy nutrient status (Peñuelas and Filella, 1998). The position of the red-edge is defined as *the wavelength where the derivative (the slope) of the reflectance as a function of wavelength is maximum* (Horler et al., 1983). As nutrient deficits increase, the red-edge tends to shift toward shorter visible wavelengths. The steep increase in reflectance marks the transition between the photosynthetically important visible wavelength region where incident light is absorbed primarily by the leaf, and a second region at longer wavelengths in the NIR where incident light is scattered primarily by the leaf. In the (visible) wavelength region 0.4 to $0.7 \mu\text{m}$, leaves typically absorb between 75 and 95% and reflect 2 to 15% of the incident light. At wavelengths longer than $0.75 \mu\text{m}$, leaves typically absorb only 5 to 10% and reflect 40 to 50% of the incident light. Because the red-edge is the side or shoulder of the chlorophyll absorption well centered near $0.68 \mu\text{m}$, as absorption increases, the shoulder shifts toward longer wavelengths. When leaf concentrations of a key nutrient decrease and absorption decreases, causing an increase in reflectance, the position of the red-edge shifts toward shorter wavelengths. Thus, the position of the red-edge provides an indication of the amount of light being absorbed by chlorophyll, which provides an indirect indication of plant nutrition levels (Filella and Peñuelas, 1994). Gitelson et al. (1996) present striking results estimating chlorophyll concentrations in maple and horse chestnut leaves. The position of the red-edge approaches $0.68 \mu\text{m}$ in the visible wavelength region as the concentration of viable chlorophyll approaches zero. Under such conditions, a normally green leaf may appear white or faintly yellow. It must be emphasized that an observed shift in the red-edge position of the reflectance of a leaf toward shorter wavelengths indicates only that viable chlorophyll concentrations in the leaf have decreased. In the absence of *a priori* knowledge, this could be caused by various nutrient deficiencies, water deficits, and even extreme temperatures.

Unlike canopy reflectance, the position of the red-edge has proven relatively insensitive to the reflectance of most soils when applied to monitor nutrient deficiencies in crop canopies. This is because the nadir canopy reflectance at wavelengths around $0.72 \mu\text{m}$ is, approximately, the weighted sum of the soil reflectance and the foliage reflectance. For wavelengths in the neighborhood of the red-edge, the derivative of the canopy reflectance has a maximum value determined largely by the very steep slope of the foliage reflectance curve rather than the more gently sloping soil reflectance curve. This means that the position of the red-edge is determined primarily by the spectral properties of the foliage, not those of the soil.

However, changes in such canopy biomass variables as LAI and the amount of scattered light do affect the position of the red edge of a crop canopy (see Figure 12.8 and work by Horler et al., 1983). This suggests care in using the red-edge position both to make comparisons between different crops and to make temporal

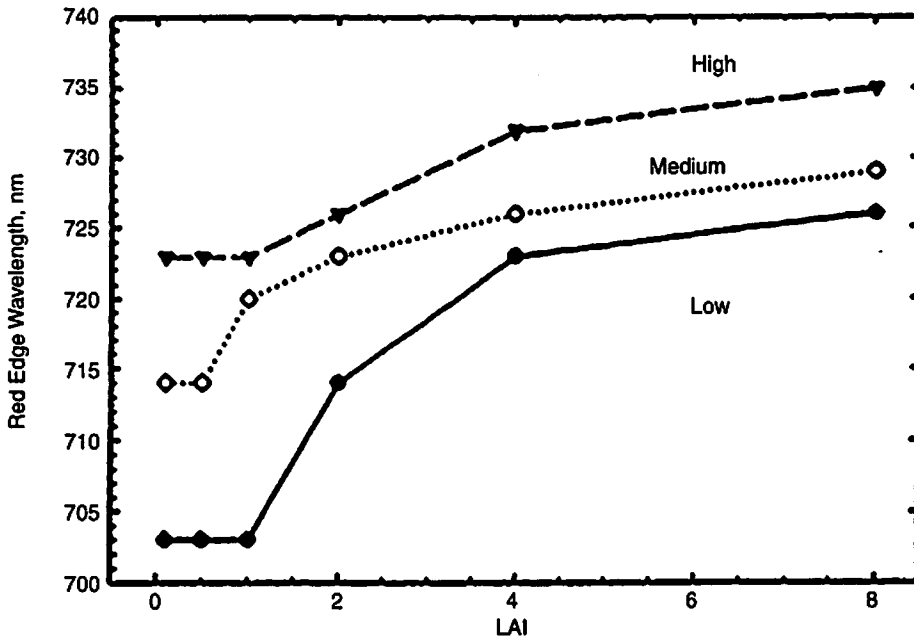


Figure 12.8 Change in the red-edge position as a function of LAIs and leaf chlorophyll concentration. (From Daughtry et al., 2000.)

comparisons of the nutrient status of a crop canopy during its vegetative growth phase when both canopy biomass and the amount of light scattered in the canopy increase rapidly. Presumably if biomass and scattering effects are accounted for, the position of the red-edge of a canopy provides an indication of canopy chlorophyll status, and indirectly its nutritional status, while being largely unaffected by the spectral properties of most soils. Dawson (2000) investigated the potential for estimating canopy chlorophyll content from analysis of data obtained from the satellite-borne MERIS sensor, with the hope that mapping the red-edge position over large regions would prove feasible.

Compared to other approaches to monitoring the nutritional status of a crop, the use of the red-edge position appears to receive consistent attention from the research community and is perhaps the most popular method at present (Munden et al., 1994; Peñuelas et al., 1994; Pinar and Curran, 1996; Blackburn, 1998b; Tsai and Philpot, 1998; Jago et al., 1999). For example, the canopy chlorophyll content index (CCCI) (Clarke et al., 2001) detects chlorophyll content based on red-edge reflectance (720 nm central wavelength, 10 nm bandwidth) compared to near-infrared reflectance (790 nm central wavelength, 10 nm bandwidth) and normalized for variation in canopy density, which was estimated using the NDVI. In the CCCI image presented in Figure 12.9, boxes were drawn around low-nitrogen plots that had received half of the recommended nitrogen level (112 kg N/ha, compared to 222 kg N/ha in the other plots), and a low CCCI value corresponds to low canopy chlorophyll content. The CCCI was able to detect the low-nitrogen treatments earlier in the season than was a standard vegetation index (e.g., NDVI) and did not

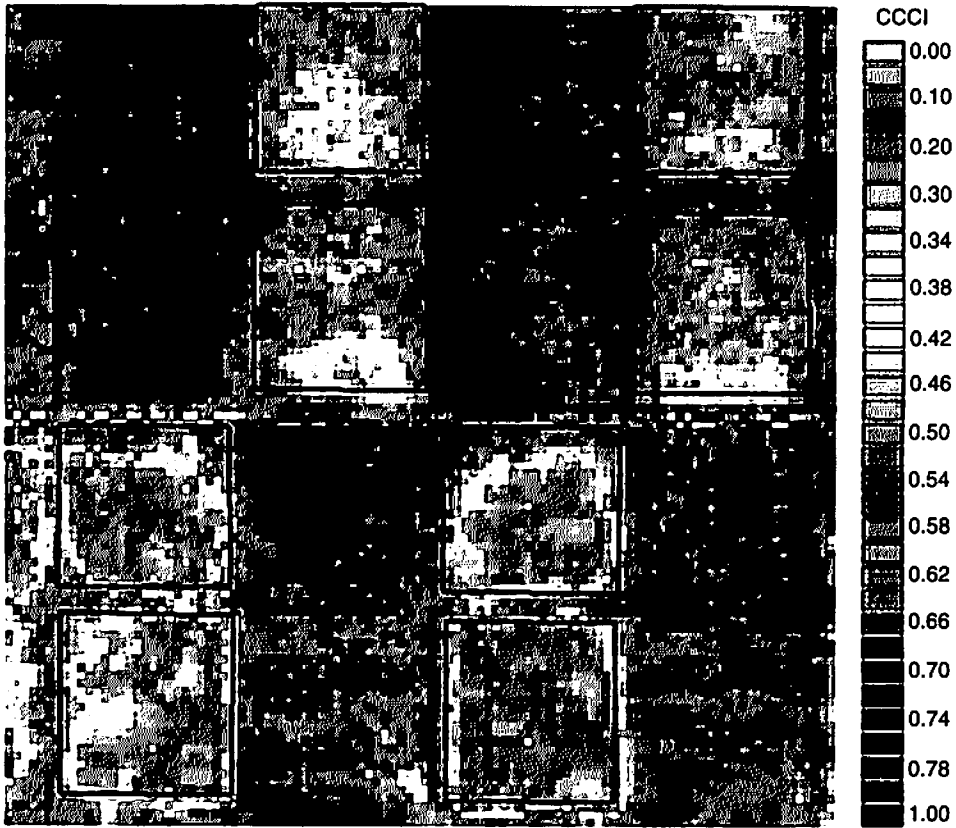


Figure 12.9 Canopy chlorophyll content index (CCCI) image of an Arizona cotton field based on red-edge reflectance (720 nm central wavelength, 10 nm bandwidth) acquired September 3, 1999 from a scanning radiometer mounted on a linear-moving irrigation system. See Barnes et al. (2000) for additional experimental details and see CD-ROM for color image.

show sensitivity to decreased canopy density resulting from low-water treatments also imposed on the field.

12.3.2.3 VEGETATION INDICES FOR DETERMINING NUTRIENT STRESS

Remote sensing methods for monitoring the nutrient status of irrigated crops often involve the use of a vegetation index (VI). Vegetation indexes have been developed and investigated for their ability to provide information about the remotely sensed scene, often by enhancing sensitivity to desirable sources of variation in the scene. Much of the research has involved two basic types of vegetation index: ratios of reflectance at two wavelengths [e.g., the simple ratio (SR) vegetation index] and normalized difference indexes (e.g., NDVI) that are generally differences of reflectances divided by the sum of reflectances. SR and NDVI have been tied to levels of fertilization, chlorophyll concentrations, LAI, and the PAR absorbed (APAR) by a crop (e.g., Walburg et al., 1982; Daughtry et al., 1992, 2000). General disadvantages of these indexes are their sensitivity to the reflectance of the soil underlying a crop canopy and the light-scattering properties of aerosol particles in the atmosphere.

The soil-adjusted vegetation index (SAVI) (Huete, 1988), the atmospherically resistant vegetation index (ARVI) (Kaufman and Tanré, 1992), the global environmental monitoring index (GEMI) (Pinty and Verstraete, 1992), and modifications to these VIs (Rondeaux et al., 1996) have been proposed in attempts to retain in the VI the dependence on plant properties while minimizing variation in the VI attributable to the effects of the underlying soil, the intervening atmosphere, and both.

Numerous vegetation indexes have been proposed for estimating the concentration of chlorophyll in a leaf or canopy. While a consensus method for estimating the chlorophyll concentration of leaves is desired within the community, the research results for canopies appear less robust and somewhat experiment specific. The following attempts to present the theoretical underpinnings of selected research results for VIs of both leaves and canopies.

For vegetation indexes computed as ratios of leaf reflectance, results reported by Gitelson and Merzlyak (1996, 1997, 1998) illustrate key concepts (Figures 12.10 and 12.11). Not only does the spectral reflectance of a leaf depend on its chlorophyll content, but in addition, the standard deviation of the leaf reflectance is a pronounced function of wavelength. Data in Figures 12.10 and 12.11 show peaks near $0.7 \mu\text{m}$ and between 0.55 and $0.6 \mu\text{m}$ and minima in the two chlorophyll absorption bands as well as in the NIR wavelength region in which chlorophyll does not absorb light. These results and others (see, e.g., Datt, 1999; Daughtry et al., 2000) show

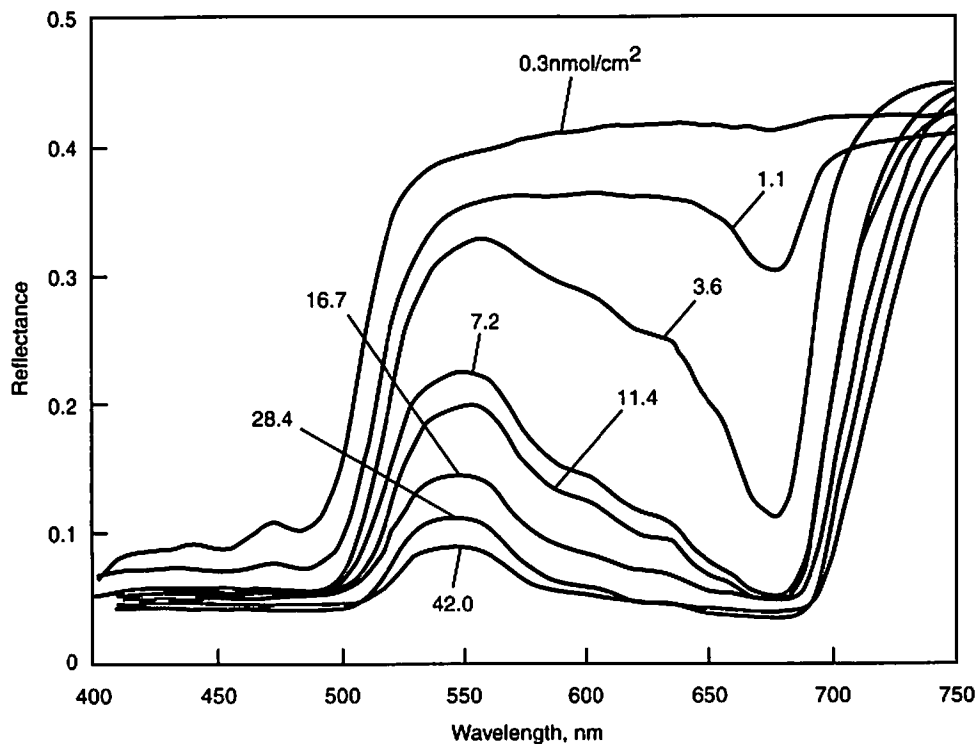


Figure 12.10 Representative reflectance spectra of maple leaves containing various concentrations of pigments. Chlorophyll *a* concentrations in nmol/cm^2 are indicated at reflectance curves. (From Gitelson and Merzlyak, 1996.)

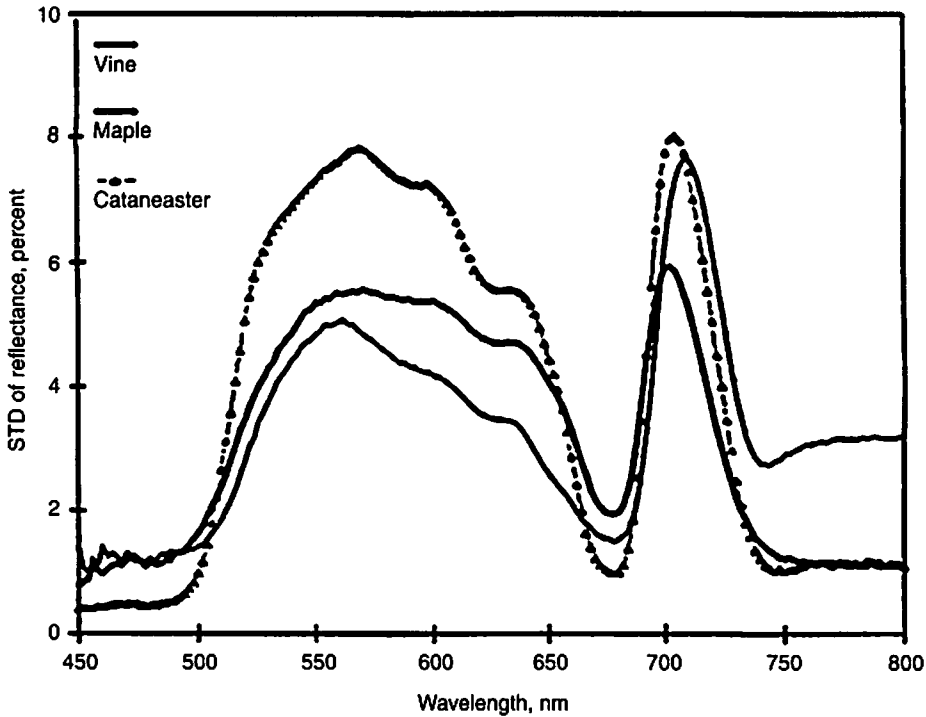


Figure 12.11 Standard deviation of reflectances for diverse plant species with total chlorophyll content of more than $5 \mu\text{g}/\text{cm}^2$ (yellowish-green to dark-green leaves). Two maxima characterize these relations: a broad curve over the green range of the spectrum from 530 to 630 nm and a narrow peak in the red range near 700 nm. Reflectance in the red chlorophyll *a* absorption maximum near 670 nm is virtually insensitive to chlorophyll variation. (From Gitelson and Merzlyak, 1997.)

that once the concentration of leaf chlorophyll increases above a relatively low level, most light incident on the leaf at a wavelength of $0.68 \mu\text{m}$ is absorbed and comparatively little is reflected. The results support the concept that increases in leaf chlorophyll content manifest changes in the leaf reflectance primarily on the shoulders of the absorption wells rather than at the center wavelength of the well, except when leaf chlorophyll concentrations are uncommonly low. The results shown in Figure 12.12 illustrate the link between leaf chlorophyll concentrations and leaf reflectance near 0.7 and $0.55 \mu\text{m}$. Application of a leaf reflectance model by Baret et al. (1988) as described in Peñuelas et al. (1995) shows that a ratio of reflectances (i.e., the leaf reflectances measured outside the absorption band at a wavelength of $0.75 \mu\text{m}$, divided by the reflectance on the shoulder of the absorption well at a wavelength of either 0.7 or $0.55 \mu\text{m}$) may be employed in a linear equation to estimate total chlorophyll ($a + b$) concentrations in the leaf (Figure 12.13) (Merzlyak et al., 1997; Gitelson and Merzlyak, 1998). For higher leaf chlorophyll concentrations, the predicting equation changes from linear to exponential. The exact spectral location of the out-of-band reflectance may not be critical, provided that it is within the NIR plateau spectral region, a suggestion supported by the leaf correlation results of Blackburn (1999). Several other vegetation indices depend on the

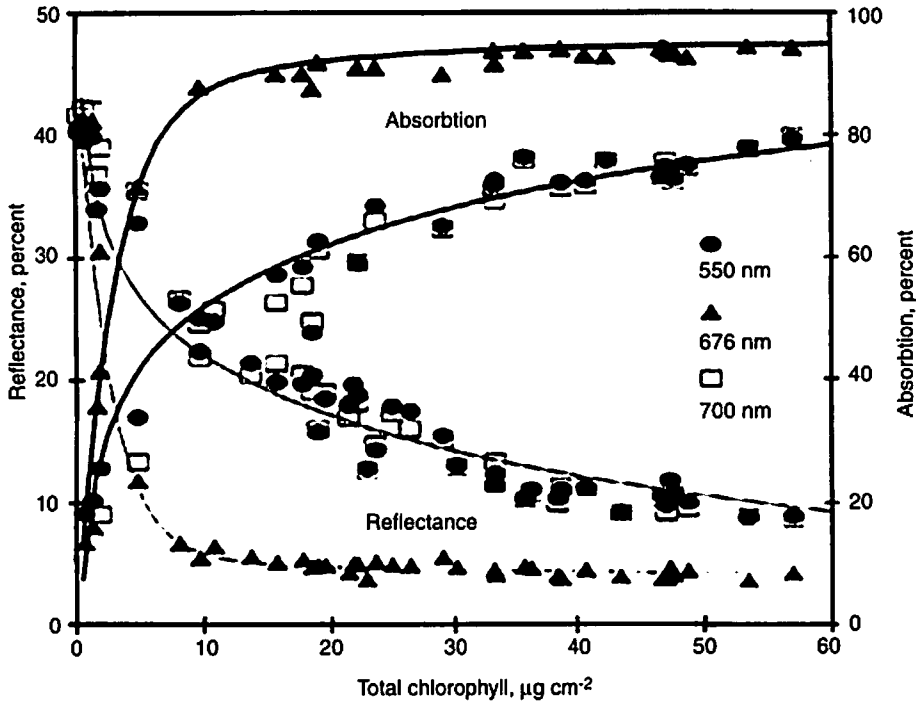


Figure 12.12 Absorption and reflectance versus total chlorophyll content in maple leaves at 550, 676, and 700 nm. Whereas reflectance and absorption at 676 nm is sensitive to low chlorophyll contents (up to $5 \mu\text{g}/\text{cm}^2$) and becomes saturated at moderate contents (for yellowish-green to dark-green leaves), at 550 and 700 nm both variables are sensitive to chlorophyll content within a wide range of its variation. (From Gitelson and Merzlyak, 1997.)

same theoretical approach. Both Chappelle et al. (1992) and Blackburn (1998a) offered ratios of reflectances at various wavelengths for estimating concentrations of chlorophyll *a* and *b* and carotenoid pigments. Schepers et al. (1996) found a quadratic relationship with an r^2 value of 0.99 between the nitrogen status of corn leaves and the ratio of leaf reflectances measured at wavelengths of 0.55 and 0.85 μm . The simple ratio (SR) can be expected to be relatively insensitive to all but very low leaf chlorophyll concentration levels if it is defined using a narrow wavelength band centered at 0.68 μm . However, it presumably would be sensitive to a larger range of chlorophyll concentrations if defined using a broad wavelength band that includes portions of the reflectance shoulders around 0.7 or 0.6 μm .

For leaves, several normalized difference-type vegetation indexes have been investigated for their ability to estimate leaf chlorophyll concentrations. Like the SR vegetation index, the NDVI, if defined using a narrow band centered near the chlorophyll absorption band near a wavelength of 0.68 μm , shows sensitivity to atypically low canopy chlorophyll (Gitelson and Kaufman, 1998). Sensitivity to a much larger range of leaf chlorophyll concentrations has been demonstrated for the green NDVI, defined as $(\text{NIR} - \text{green})/(\text{NIR} + \text{green})$ (Gitelson et al., 1996; Gitelson and Kaufman, 1998; Gitelson and Merzlyak, 1998). Gitelson et al. (1996) showed the atmospheric-resistant green index (GARI) and atmospheric-resistant green-red

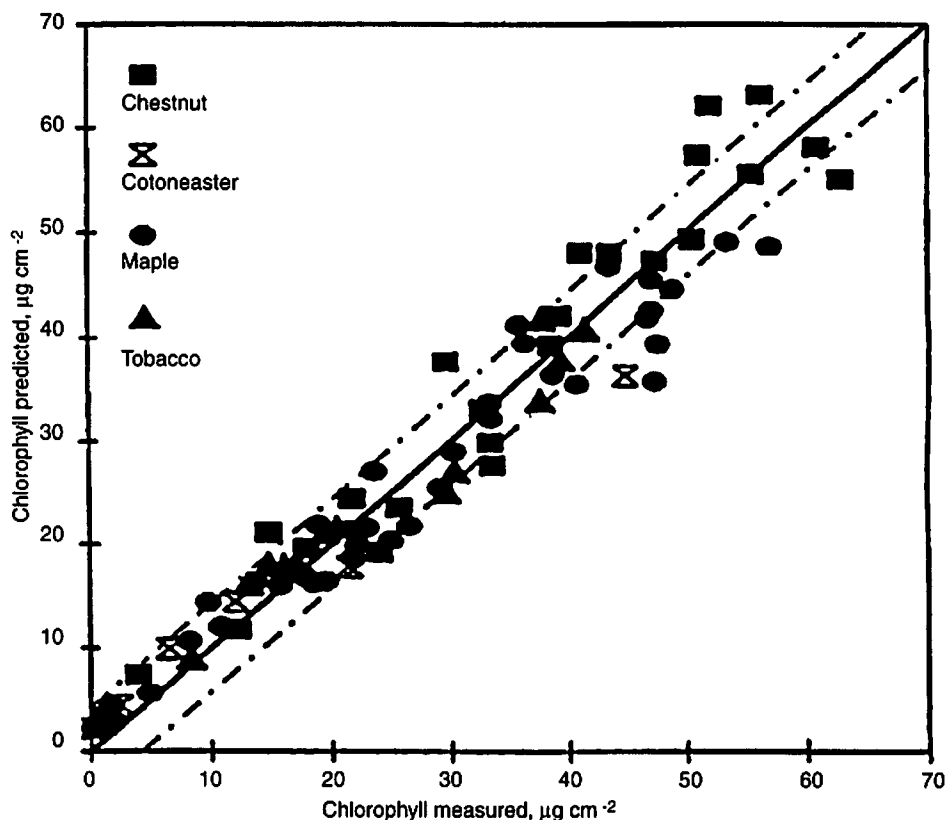


Figure 12.13 Results of validation of a ratio of reflectance at 750 and 700 nm (R_{750}/R_{700}) by model-testing subset (96 leaves of maple, chestnut, tobacco, cotoneaster, vine, and fig). The correlation between predicted and actually measured chlorophyll content was $r^2 = 0.94$; an error of chlorophyll content prediction of $4.06 \mu\text{g}/\text{cm}^2$ was achieved. The solid line represents the 1:1 line and the dotted lines represent error or chlorophyll prediction. (From Gitelson and Merzlyak, 1997.)

index (GRARI) to be much more sensitive to chlorophyll concentrations than either NDVI or ARVI, but he did not validate them using canopy data.

At the canopy scale, few image-based efforts have been reported with the goal of developing robust, VI-based methods for estimating the nitrogen status (chlorophyll concentration) of a crop canopy. In one recent investigation, GopalaPillai and Tian (1999) collected digital imagery in three wide wavelength bands (green, red, and NIR) over nitrogen-stressed corn. Their analysis of the uncalibrated imagery using clustering, correlation, and the NDVI and SR vegetation indexes found that the VI provided a better indication of crop nitrogen stress than did the uncalibrated image gray-level values.

In theory at the canopy scale, estimates of the chlorophyll concentration per unit ground area depend on two factors: the chlorophyll concentration per unit leaf area (which leaf-scale vegetation indexes conceivably could provide) and the leaf area per unit ground area [leaf area index (LAI)] of the canopy (Blackburn, 1998b). Thus, to provide estimates of canopy chlorophyll concentrations, a canopy scale vegetation index must vary with changes in leaf scale chlorophyll concentrations and must

respond to changes in the canopy LAI. However, without experimentation, it is not clear that one VI can be applied with equally high success to estimate chlorophyll concentrations in both leaves and canopies.

Canopy reflectance at wavelengths 0.68 μm , 0.72 μm , and the NIR plateau appears likely to contain the information needed for estimating canopy chlorophyll concentrations. Results from several studies have confirmed that canopy reflectance in the red and NIR plateau is highly correlated with LAI (see Figure 12.14 and work by Walburg et al., 1982). As Gitelson and Kaufman (1998) note, for chlorophyll concentrations above a threshold value, leaf reflectance at 0.68 μm is essentially a constant, displaying little variability with changes in leaf chlorophyll concentrations. This explains why canopy LAI may be estimated successfully from vegetation indexes defined using canopy reflectances at 0.68 μm and NIR plateau wavelengths (Daughtry et al., 2000; Thenkabail et al., 2000). Near a wavelength of 0.72 μm , the correlation between canopy LAI and canopy reflectance changes from negative in the red spectral region to positive in the NIR plateau spectral region (Figure 12.14) and is therefore identically zero at one wavelength, here denoted λ_{lc} . Canopy reflectance is unaffected by variations in LAI at this wavelength, which varies slightly with crops such as cotton, potato, soybean, corn, and sunflower (Figure 12.14). If we assume that soil reflectance does not affect canopy reflectance, then at the wavelength λ_{lc} , canopy reflectances contain information about the concentration of leaf chlorophyll rather than information about both leaf chlorophyll concentration and canopy LAI.

The location of λ_{lc} depends primarily on the magnitude of the reflectance and transmittance of canopy components and secondarily, on the amount of light scattered between canopy components, which in turn depends on canopy architecture. Thus, as the chlorophyll concentration of canopy components decreases, the reflectance and transmittance of canopy components increases and the position of λ_{lc} would shift toward the center of the chlorophyll absorption well at a wavelength near 0.68 μm . If leaf chlorophyll concentrations are uncommonly low, correlation

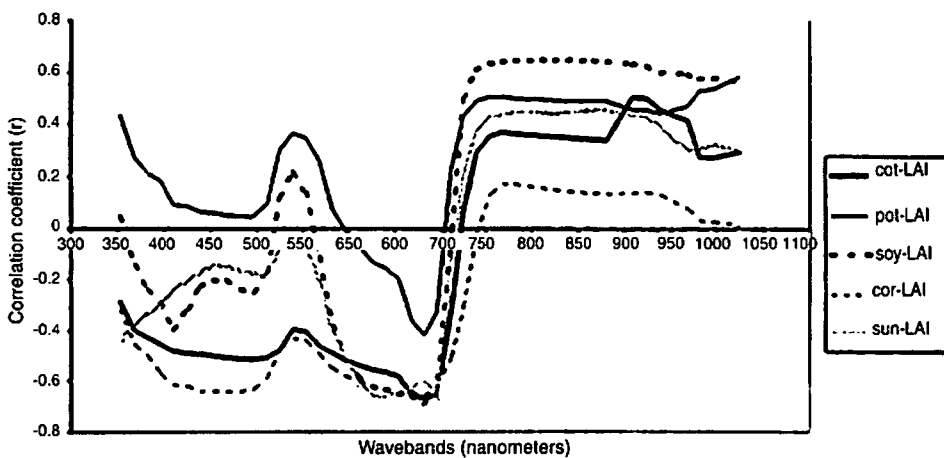


Figure 12.14 Correlation coefficients (r) between spectral reflectance in 512 discrete spectral channels and biophysical variables of five crops for LAI. (From Thenkabail et al., 2000.)

between canopy reflectance and LAI would probably be positive even at a wavelength of $0.68 \mu\text{m}$ and λ_{1c} could not be defined. In all probability, the location of λ_{1c} for leaf chlorophyll concentrations more typical of crop canopies would be in the wavelength range 0.7 to $0.74 \mu\text{m}$, thus facilitating design of measuring instruments. In addition to λ_{1c} , the correlation between canopy reflectance and canopy chlorophyll concentrations is often reduced in the green wavelength region (e.g., Blackburn, 1998b).

Thus, estimates of canopy reflectance at $0.68 \mu\text{m}$, $0.72 \mu\text{m}$, and a wavelength in the NIR plateau would appear potentially to contain the information necessary for estimating both the leaf chlorophyll concentration and the canopy LAI. Further, using those estimates, an estimate of the canopy chlorophyll concentration could be obtained. How the influence of the soil reflectance upon canopy reflectances at λ_{1c} could be minimized is not evident if the field of view of the sensor includes vegetation and soil. However, perhaps a reflectance mixture analysis might prove successful (Ustin et al., 1993).

12.3.2.4 IMAGING SYSTEMS FOR DETECTING CROP NUTRIENT STRESS

Only a few digital image-based research studies have been reported that estimate within-field nitrogen/chlorophyll status of agricultural crop canopies. Nevertheless, the rapidly emerging, relatively low cost digital imaging technology is potentially more capable of meeting the information needs of site-specific agriculture than are photography-based approaches. Lamb (2000) reviewed the potential uses of digital imaging technology in agriculture in southeastern Australia, providing examples demonstrating its applicability to not only assessing crop nitrogen status but also to inferring certain soil characteristics, detecting weed infestation, and estimating crop yields. Munden et al. (1994) and Jago et al. (1999) analyzed hyperspectral CASI image data collected over winter wheat, estimating canopy chlorophyll concentrations from the position of the red-edge. From analysis of uncalibrated digital imagery collected in green, red, and NIR wavelength bands over nitrogen-stressed corn, GopalaPillai and Tian (1999) found that the NDVI and SR vegetation indexes provided a better indication of crop nitrogen stress than did the uncalibrated image gray-level values. LaCapra et al. (1996) applied the techniques of imaging spectroscopy (also termed imaging spectrometry and described in a review by Green et al., 1998) to analysis of hyperspectral airborne visible/infrared imaging spectrometer (AVIRIS) data (Vane et al., 1993), estimating nitrogen concentrations in rice fields from regressions involving radiances measured in narrow spectral bands. Band selection was based on correlograms of laboratory absorption spectra. More often, application of the techniques of imaging spectroscopy has yielded estimates of nitrogen concentrations in forest canopies (Wessman et al., 1988; Zagolski et al., 1996; Martin and Aber, 1997). Many studies have achieved success in remotely estimating foliar nitrogen despite a striking lack of consensus on which spectral bands in the wavelength region 1.0 to $2.5 \mu\text{m}$ to include in the estimation process (LaCapra et al., 1996).

Remote sensing research during the last 45 years has often taken advantage of the capability of photographic imagery collected from aircraft to provide a synoptic view of the within-field spatial variability of an agricultural crop. Some of the more recent investigations involving nitrogen fertilization include those of Blackmer and

Schepers (1996) and Blackmer et al. (1996). They related density variations within airborne imagery collected over fields of corn in reproductive growth and digitized in the blue, green, and red wavelength regions, to within-field differences in both the nitrogen status and ultimate grain yield. Blackmer and Schepers (1996) were able to predict grain yield with an r^2 value of 0.93 from analysis of imagery representing a narrow band centered at 0.536 μm . Moragham (1998) used color photographs of a sugar beet canopy taken prior to harvest to identify green, yellow-green, and yellow areas of the field, suggestive of high-to-low variation in concentrations of plant chlorophyll and soil nitrogen. Subsequent analysis showed corresponding variation in the concentration of nitrogen in sugar beet tops, leaves, and the upper 1.2 m of soil, although nitrate-nitrogen in the sugar beet tops was partially responsible for the higher nitrate-nitrogen at the green sites. Moragham (1998) concluded that aerial photography and GPS technology can increase the precision of soil testing for nitrogen and decrease subsequent nitrogen fertilizer use if a variable-rate applicator is used.

Use of color infrared film allows measurement of the visible green and red wavelength regions in which film response is related to biomass and leaf chlorophyll concentrations, as well as the NIR region out to a wavelength of approximately 0.8 μm , where the film again responds to the amount of canopy biomass. Plant et al. (2000) found a significant correlation between ultimate lint yield and the time integral of the NDVI determined from digitized aerial color infrared photographs of replicated cotton plots exhibiting varying levels of water and nitrogen stress sufficient to affect yield. Analysis of within-field nutrient variability using aerial photography exploits its advantages (virtually instantaneous measurement of the visible and near-infrared wavelength regions, synoptic view, and high spatial resolution), while not depending on calibration, which can be problematic with film, especially if the film is from different manufacturing lots. Although film calibration is potentially an important issue in temporal studies, Plant et al. chose not to calibrate after comparison showed a linear relationship between calibrated and uncalibrated values of NDVI. They argue that their approach allows valid comparison of NDVI values representing different locations photographed at one time, and they recognize that comparisons of NDVI between dates are invalid. In their results obtained by time integration of the NDVI values, a comparison of trends, but not specific values, is valid.

At least one tractor-mounted system has been patented for monitoring crop nitrogen status using a multispectral imaging system (Dickson et al., 2000). Data provided by such a system could be used as input to variable-rate fertilizer application systems, thereby providing the capability to correct any crop nitrogen deficiencies observed by the multispectral imaging system. In the preferred embodiment described in the patent, if mounted on a tractor, the system images an area approximately 6.1 by 4.6 m in three wavelength regions (green, red, and NIR). The system proceeds to calculate the NDVI of each pixel, derive histograms of NDVI for the image, and select a threshold value that best separates vegetation and non-vegetation. Next, it selects those pixels classified as vegetation, computes the green band reflectance of each vegetation pixel, and estimates the nitrogen level in the vegetation based on the green reflectance values. The patent also describes several other alternative methods of estimating vegetation nitrogen status.

Stone et al. (1996) and Taylor et al. (1998) describe non-imaging tractor-mounted systems developed for detecting and correcting crop nitrogen stress from multispectral radiometric measurements. In some cases, these systems allowed fertilizer inputs to be reduced by 60%.

12.3.3 Weed Scouting and Herbicide Application

The impact of weeds on reduced crop yields has been recognized for many years. Crop stress because of weed interference has been attributed to many factors, including allelopathy and competition for sunlight, soil water, and nutrients (Sikkema and Dekker, 1987). Currently, information about weed density and distribution is difficult to obtain, due to time and labor of rigorous scouting, the complexity of interpreting scouting information, the assumption that weeds are constant and uniform throughout a field, and the lack of equipment to manage weed variability easily. Consequently, uniform applications of herbicide are determined for a field based on last year's weed problems or information obtained from scouting field edges. Such broadcast herbicide applications have been successful in controlling weeds and improving profits when weeds are randomly or uniformly distributed in the field. However, in most cases, weeds are highly aggregated in a field (e.g., Johnson et al., 1995a; Cardina et al., 1996).

Studies have shown that drainage, topography, soil type, and microclimate play important roles in weed distribution and weed competition with crops at specific sites, resulting in significant variation in weed densities across individual fields (e.g., Wiles et al., 1992). As a result, site-specific weed management could be valuable, and in fact, studies have shown that this management strategy has reduced herbicide use by 40 to 60% without affecting crop yield (Brown and Steckler, 1995; Johnson et al., 1995a).

The potential savings associated with site-specific weed management have stimulated the development of high-technology systems for managing weed variability. A good example is the Map 'N Zap System, which utilizes a map of weed patches to generate a traversal pattern representing the planned path of the tractor through the field (Nuspl et al., 1996). For weed patches 60 to 100 m in length, Map 'N Zap tells the injection system the type and amount of chemicals to be injected and sprayed.

Remote sensing has been proposed as a component of integrated systems for management of weeds. Brown and Steckler (1995) described a system that combined image-derived weed maps with a GIS-based decision model to determine optimum herbicide mix and application rates for no-till corn and resulted in reductions of herbicide use by more than 40%. In an economic analysis, Wiles and Schweizer (1999) found that the most expensive component of such integrated systems is creating the maps of the weed population in a field. They suggested that valuable information about the distribution of a weed population in a field may be obtained from remote sensing.

The remote sensing methods for providing early and late season information for high-technology weed management systems are different, as described in the following subsections. This difference is due primarily to the fact that herbicides are applied both prior to planting and postemergence, and postemergence applications are

generally based on weed population maps produced no later than eight weeks after planting.

12.3.3.1 EARLY-SEASON WEED DETECTION

The information requirement for preplant or early-season herbicide application is simply determination of the presence or absence of plants. In some cases, this is also the requirement for management of weeds growing between crop rows at early crop growth stages (e.g., Pollet et al., 1999). Remote sensing systems designed for such weed detection generally use the reflectance differences between relatively wide spectral bands in the visible and NIR spectra to make the distinction between plants and soil or rock. Such a simple sensor has been used to measure the status of the crop, and at the same time to detect and evaluate the degree of weed leaf area between the rows by image analysis (Heisel and Christensen, 1999). Medlin et al. (2000) found that remote sensing could detect weed infestations of 10 plants/m² or more with at least 90% accuracy. This level of accuracy could be very beneficial for directing weed scouting practices and for determining the area occupied by weeds.

Many of these simple systems are tractor- or aircraft-based, to achieve the desired spatial and temporal resolution. Despite reported successes, most studies have also reported difficulty in discriminating the effects of soil variability on the reflectance properties of soils, crops, and weeds (Medlin et al., 2000). Measurements become even more difficult to interpret due to variations in solar intensity and sun-sensor-surface geometry. The latter problem has been partially circumvented in some tractor-based systems through scene illumination with a controlled light source, such as a broadband 100-W halogen lamp (Feyaerts et al., 1999).

12.3.3.2 LATE-SEASON WEED DETECTION

Management of post-emergence herbicide applications poses more difficulty because it requires discrimination between weeds and crops. This is generally accomplished by using the difference between spectral signatures of crops and specific weeds or by acquiring images at specific times during the season when weed coloring is particularly distinctive (i.e., during flowering) or weed patches are comparatively large, dense, and/or tall. The accuracy of such approaches generally increased during late-season growth stages, due to increased ground cover of weed species. Remote sensing systems for discriminating crop-weed spectral signatures or monitoring weed color are usually filtered to multiple, and relatively narrow, spectral bands in the visible and NIR spectra.

There is evidence that it is possible to make a distinction between crops and weeds based on small differences in the spectral signatures, particularly with high-spatial-resolution imagery (e.g., Feyaerts et al., 1999; Pollet et al., 1999). The success of this approach is variable, depending on the weed and crop species and phenologic stage. The greatest success has been achieved when the weed species dominated the crop or the weed was flowering and the color differences were greatest (Brown et al., 1994). Thornton et al. (1990) were able to discriminate weed patches at the flowering stage in a winter cereal field from their color on aerial photos. Christensen et al. (1999) showed that weed leaf area measured with an image analysis technique could be used to map and stratify weed sampling.

Other successful approaches have focused on the separation of cereal crops and dicotyledon weeds using video imagery (e.g., Zhang and Chaisattapagon, 1995).

Brown et al. (1994) used a multispectral still video camera from a low-flying (500 to 700 m) aircraft and a ground-based vehicle (10 m aboveground) to detect patches in a cornfield of seven common dicot and monocot weed species. They found that the species could be fairly well discriminated by their spectral characteristics of reflectance at four wavelength bands, but weed and crop features were strongly variable with growth stage.

Pérez et al. (2000) proposed a combined image analysis in which spectral reflectance was used to discriminate between vegetation and background, and shape analysis techniques were applied to distinguish between crop and weeds. The results were compared with an interpreter-based classification, providing an acceptable success rate. They suggested that these results would be most useful in a stratified manual weed survey of the field.

As an alternative to measurements of surface reflectance, some studies have investigated the use of TIR measurements to monitor the crop water deficiency and stomatal closure associated with the competition between weeds and crops for soil water. Sikkema and Dekker (1987) found that daily infrared thermometric monitoring of soybean leaf temperature could be used to identify critical periods of weed-induced stress. However, soybean growth and potential yield in the weedy plots had already been affected before high leaf temperatures were first noticed. Therefore, the use of this technique had more value in monitoring the timing of such stress periods than as an advance warning tool.

12.3.3.3 COMBINED APPROACHES FOR WEED DETECTION

Most approaches presented earlier for mapping and monitoring weeds have been based solely on spectral information. In fact, there is great potential to combine spectral images with ancillary information to improve results. There is general agreement that spatially heterogeneous weed populations are rather stationary over time, although weed emergence varies between years (Gerhards et al., 1996). Christensen et al. (1999) suggested using historical weed maps to divide the field into weed zones, where manual weed surveying could be carried out. In fact, since perennial weeds tend to remain in the same location each year, there is even the possibility of using the previous year's weed map for pre-plant control decisions (Brown and Steckler, 1995).

The results of most spectral analyses is a map of the *total* leaf area of weeds; however, the total weed leaf area may not reflect the impact of the weeds when the species have different growth rates or growth habits. If maps of weed species could be derived from information about total weed leaf area, these maps could be combined with decision models to optimize the herbicide selection and dose for a mixture of weed species. A weed management model for patch spraying was described by Heisel et al. (1996), using a map of weed species to determine competition between crop and weed mixtures, herbicide performance, and economic optimization of herbicide dose. The general weed management (GWM) model uses weed species and density as input parameters and a list of herbicide options based on predicted net return to generate an estimate of application efficacy (Broulik et al., 1999).

12.3.4 Insect Scouting and Insecticide Application

Due to the spatial resolution of current air- or spaceborne imaging systems, it is unlikely that one could use remote sensing to directly observe insects and other pest organisms affecting plants as part of an operational crop monitoring program. Rather, use of remote sensing in this regard usually involves one of the following activities: (1) observing the extent of damage to crops caused by insects or other pests to facilitate the assessment of yield, (2) observing plant canopy conditions in fields that might be conducive to the development of infestations by insects or other crop pests, or (3) observing the early stages of infestations by insects or other crop pests in fields for the purpose of initiating control measures.

The production of crops under irrigated conditions tends to result in a field environment that favors the proliferation of insects and other pests that damage crops. To date, most of the research in these areas has involved major field crops such as grains and cotton. Techniques developed in these studies, however, are applicable to a wide variety of agricultural crops, including tree crops, vines, and vegetables.

The use of remote sensing observations of pest-related crop damage to facilitate yield assessment is an after-the-fact application of this technology. It occurs when measures to control pests have been neglected or are inadequate, or when the use of control measures was not considered economical. Use of remote sensing in assessing crop yield is discussed in detail in a separate section.

12.3.4.1 MANIFESTATIONS AND MANAGEMENT OF INSECT INFESTATIONS

A reasonable strategy for controlling insects and other crop pests in fields is to anticipate their presence based on the occurrence of conditions in the plant canopy that represent a favorable habitat for these organisms. This concept can be illustrated by the following examples:

- It has been observed that the tarnished plant bug (*Lygus lineolaris*) is attracted to areas within cotton fields that contain the most lush, vigorous plant growth. Researchers from NASA, USDA, and several universities used airborne multispectral imagery to map these areas within cotton fields in Louisiana to indicate where infestations of this insect should occur. Areas with lush, vigorous plant growth were indicated by relatively high values of NDVI derived from the remote sensing image data. These portions of the cotton fields were more extensively scouted for the occurrence of this pest, and the maps derived from the remote sensing imagery were used to direct spatially variable insecticide applications (Willers et al., 1999, 2000).
- In cotton fields in the Rio Grande Valley of Texas, overwintering of the boll weevil (*Anthonomus grandis*) is controlled by plowing stalks and unopened bolls into the soil following harvest in the fall. Regulations dictate that all cotton fields in this region must be "plowed down" by a specified date, since fields that escape this management practice represent favorable habitats for overwintering of this pest. Researchers from USDA demonstrated the use of airborne multispectral videography and SPOT satellite imagery to monitor farmer compliance with this regulation. Cotton fields that had not been plowed down could

be discriminated from those that had using false-color composite imagery from these remote sensing systems (Richardson et al., 1993).

An important benefit of this approach is to direct ground-based crop scouting activities to fields or portions of fields where insects or other pests are most likely to be found. Since ground-based scouting is time consuming and labor intensive, reduction in the overall effort through directed scouting could reduce the cost to farmers for this necessary operation.

If an infestation of insects or other crop pests could be detected while its areal extent was limited to a small fraction of the field, only that portion of the field might be sprayed with pesticide. Such a spatially variable strategy of "spot treatment" could have a number of advantages over conventional field spraying, including reducing the total amount of pesticide applied to the environment and maintaining populations of beneficial insects and arthropods outside the infested portion of the field. For this strategy to be effective, infestations typically need to be detected in their earliest stages of development. Accomplishing this through remote sensing would probably require frequent high-resolution imagery, such as that currently obtained using aircraft-based systems.

Pest organisms can affect crop plants in various ways. Insects such as the boll weevil attack only the fruiting organs, leaving the foliage of the plant unaffected. Since the remote sensing signal from crop plants is dominated by foliage effects, remote sensing would be relatively ineffective in detecting early infestations of pests of this type. However, many pest organisms do affect the foliage of crop plants, either by consuming leaf tissue directly or by sucking sap from the plant, resulting in loss of leaf turgor (and possibly increase in leaf temperature) or leaf necrosis and senescence. In some cases, pests such as the glassy-winged sharpshooter (*Homalodisca coagulata*) can introduce diseases into crop plants, resulting in leaf and plant mortality. Remote sensing can potentially be effective in detecting infestations of insects or other pests that affect crop foliage.

12.3.4.2 REMOTE SENSING FOR DETECTION OF INSECT INFESTATION

In situations where early infestations are accompanied by leaf senescence or mortality, remotely sensed measures of plant canopy density such as NIR reflectance or NDVI can be effective in their detection. Decline and mortality of grape vines in California caused by the root-feeding pest *Phylloxera vitifoliae* has been monitored using NDVI derived from airborne imagery (Johnson et al., 1995b; Lobitz et al., 1996). Everitt et al. (1996) demonstrated the effectiveness of airborne NIR videography in locating areas within cotton fields defoliated by harvester ants. Another example (Wrona et al., 1998) is presented in Figure 12.15. The inset in this figure shows a small area of defoliation in a cotton field (marked with a white flag) approximately 1 m in diameter caused by an infestation of spider mites (*Tetranychus* spp.). These features, commonly called *hotspots*, represent the early stages of infestation of a field. Figure 12.15 also contains a false-color composite image (green, red, and NIR spectral bands) of the field containing this feature. This image was obtained using an airborne digital camera system at an altitude of 1524 m (5000 ft), with a resulting surface resolution of approximately 1 m. In this example, the hotspot was easily detected using remote sensing. Unfortunately, there are many

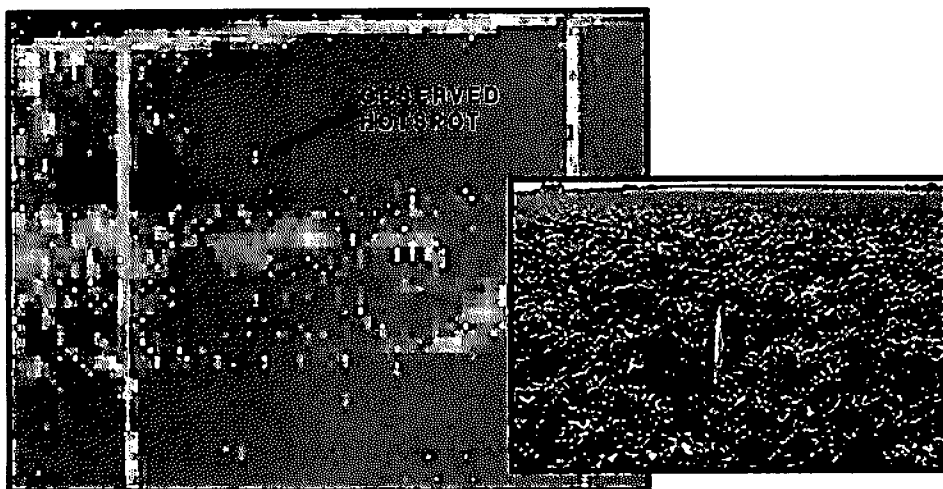


Figure 12.15 False-color airborne multispectral image of a cotton field containing a spider mite hotspot. Inset shows the hotspot (marked with a white flag) in the field. See CD-ROM for color image.

other features in this image that have the same general appearance as the hotspot, and field scouting verified that for most of them the associated reduction in canopy density was not due to insects. In this case, discrimination of one feature as an insect infestation was suggested by comparing this image with a corresponding image obtained a week earlier, in which the feature representing the hotspot was conspicuously absent. This example points out the utility of multitemporal analysis of remote sensing data for detecting transient features such as insect infestations, but it also emphasizes the associated need for frequent observations.

It has been observed that some crop pests not only physically damage the leaf canopy but also cause a change in the spectral reflectance characteristics of the affected foliage. Pinter (1994) reported from greenhouse studies that honeydew deposited on cotton leaves by feeding silverleaf whiteflies (*Bemisia tabaci*) profoundly affected the reflectance characteristics of the leaves. These effects resulted not only from the dried coating of honeydew on the leaves but also from the growth of sooty mold (*Aspergillus* spp.) supported by the coating. Aphids (*Aphididae*) can cause a similar honeydew deposition on leaves. An example is presented in Figure 12.16 (unpublished data of S. Maas), which shows leaf reflectance spectra obtained using a portable spectroradiometer and integrating sphere for cotton leaves with various degrees of honeydew accumulation and mold growth. The curves in this figure indicate that the magnitude of diffuse leaf reflectance in the visible and NIR spectral bands decreases with increasing amounts of honeydew deposition and mold growth (as indicated by the corresponding leaf photographs). This effect was most prominent in the NIR spectral band.

Remote sensing observations involving the effects of pest infestations on leaf reflectance have been described by a number of researchers. Effects of honeydew and sooty mold on leaves was reported in airborne video imagery of cotton fields in South Texas infested with whitefly (Everitt et al., 1996; Summy et al., 1997).

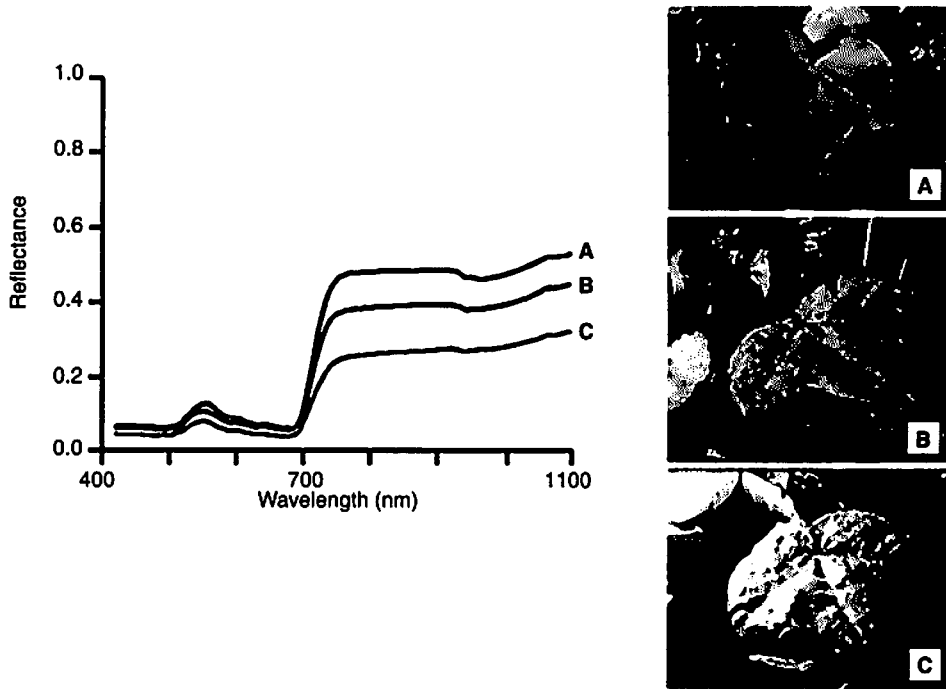


Figure 12.16 Reflectance spectra for cotton leaves with varying amounts of honeydew and sooty mold on their surface associated with aphid feeding. Leaf A is unaffected, leaf B has moderate deposits of honeydew and mold, and leaf C has heavy deposits of honeydew and mold. See CD-ROM for color image.

Everitt et al. (1994) reported similar effects in airborne video imagery of citrus trees infested with citrus blackfly (*Aleurocanthus woglumi*). Riedell et al. (2000) reported that the reflectance of wheat leaves in the spectral bands associated with light absorption by chlorophyll correlated significantly with damage caused by greenbugs (*Schizaphis graminum*) and Russian wheat aphids (*Diuraphis noxia*). Sudbrink et al. (2000) reported differences in visible and NIR reflectance between a healthy cotton canopy and one infested with two-spotted spider mite (*Tetranychus urticae*), and that mite hotspots were visible in airborne multispectral video imagery of affected cotton fields.

Maas (1998) used the NIR leaf reflectance data in Figure 12.16 in a computer simulation of the reflectance of a cotton field containing a small area of aphid infestation. In this case, the area of infestation was not readily discernible in the simulated image of the field until the contrast among brightness levels within the image was increased through computerized enhancement. Image processing can be a powerful tool in analyzing remote sensing imagery to identify possible pest infestations, as it allows subtle differences in canopy reflectance, which might normally escape the naked eye, to be magnified and made more obvious.

A number of approaches involving image processing have been reported. Examples of the some of the more sophisticated approaches include:

1. Fitzgerald et al. (1999a) used a bit-error filter in the image processing software ENVI (RSI, 1999) to enhance NIR airborne imagery of cotton fields to identify

infestations of spider mites. This filter uses an adaptive algorithm to replace the digital value of a pixel in an image with the average values of neighboring pixels. By choosing the proper threshold value, features in the image with a particular brightness characteristic can be isolated from the rest of the image. In this study, this filtering technique was used to discriminate features in the imagery associated with mite infestations from other features, including areas of the fields containing plants experiencing water stress.

2. Fitzgerald et al. (1999b) applied principal components analysis (PCA) and supervised classification to airborne imagery of cotton fields acquired in the green, red, and NIR spectral bands. In this procedure, a set of two three-band (green, red, and NIR) images acquired on different dates during the growing season was transformed using the PCA procedure in ENVI (RSI, 1999) into six principal component images that enhanced various features (e.g., water stress, soil brightness) in the image data. Training sets representing four classes (healthy plant canopy, mite-infested plant canopy, water stressed plant canopy, and bare soil) were selected within the principal component images based on field scouting. Based on these training sets, all the image data were separated into the four classes. The procedure was applied to five other pairs of three-band images acquired during the study and was generally successful at discriminating between the four classes in each pair (an example is shown in Figure 12.17).

3. Fitzgerald et al. (2000a,b) applied PCA and supervised classification to individual three-band (green, red, and NIR) airborne images of cotton fields to separate the image data into three classes: healthy plant canopy, mite-affected plant canopy, and bare soil. Change detection was then performed on pairs of classified images acquired on different dates to identify areas within the cotton fields that changed from one class to another between two dates. This procedure was able to reveal the temporal progression of mite infestation across the fields during the growing season in the remote sensing imagery.

12.3.4.3 COMBINING REMOTE SENSING AND MIXTURE MODELING FOR DETECTING INSECT INFESTATION

Image processing procedures such as those described above make use of the spectral data contained in the remote sensing imagery itself. Since soil and plant character-

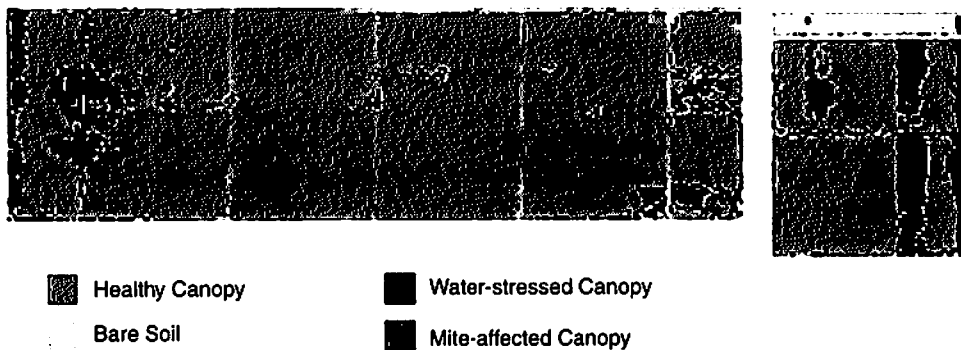


Figure 12.17 Partitioning of the surface area of two cotton fields into four classes to help identify spider mite infestations, based on the analysis of airborne multispectral imagery. See CD-ROM for color image. (From Fitzgerald et al., 1999b.)

istics may be more-or-less specific to the situation being studied, it may be difficult to achieve comparably accurate results when the procedures are applied to data acquired at different locations or times. As described earlier in this section, greenhouse and field studies involving spectroradiometric measurements indicate that some pest infestations affect the reflectance characteristics of plant leaves in specific ways. If these "spectral signatures" were consistent over space and time, it might be possible through image processing to identify their presence in multispectral or hyperspectral remote sensing imagery.

A complicating factor in this approach is that for agricultural targets, the brightness of each pixel in a remote sensing image is almost always the result of the combined reflectances of different types of surfaces (healthy leaves, infested leaves, bare soil, shadows, etc.) contained within the area of the pixel. Even with high-resolution imagery of crop canopies acquired from aircraft, it is unlikely that the reflectance of any pixel would represent a "pure" spectral signature of any surface type. Thus, practically all pixels in crop imagery are "mixed pixels." However, if the spectral signatures of the various types of surfaces within the imaged area are known, mathematical procedures can be used to "unmix" the observed remote sensing data to estimate the relative amounts of each surface type within each pixel.

The simplest and most straightforward version of this approach is linear spectral unmixing (LSU), in which it is assumed that the contribution of each spectral characteristic is in linear proportion to its relative abundance. This procedure has been incorporated into commercial image processing software such as ENVI (RSI, 1999). The user supplies spectral signatures for each of the surface types (called *endmembers* in this analysis) known to be within the area of the observed multiband remote sensing imagery. The number of spectral bands must be greater than or equal to the number of endmembers. The procedure is most successful when the spectral signatures of the endmembers are spectrally dissimilar and the observed spectral bands are relatively narrow and distributed across a wide spectral range. For this reason, LSU is particularly suited to analysis of hyperspectral image data, where the user can select imagery from among many narrow spectral bands.

Linear spectral unmixing has been applied extensively to geological studies, where libraries of the spectral signatures of many minerals are available. To date, LSU has found limited application to remote sensing studies involving insects or other crop pests. Part of the problem has been the difficulty in obtaining spectral signatures in the field. Portable spectroradiometers like those used to collect the data in Figure 12.16 are labor intensive and time consuming to use in the field. The user must be careful to ensure that the spectroradiometer is properly pointed to measure the desired surface, which in the case of pest-related studies may be only a small infested portion of a leaf. Use of an integrating sphere to measure leaf reflectance provides data only under diffuse illumination conditions and cannot directly measure the effects of nondiffuse illumination (specular reflection) or shadows on apparent leaf reflectance within a plant canopy. In recent years, the development of the liquid-crystal tunable filter (LCTF) has made the collection of spectral signatures in the field simpler (see Figure 12.18). An LCTF can be attached to a standard monochrome digital camera to step rapidly through a sequence of narrow spectral bands, allowing an image to be acquired for each band. These images can then be analyzed using standard image processing software to extract spectral data for objects (or portions of objects) appearing in the imagery. In practice, it is difficult to coregister

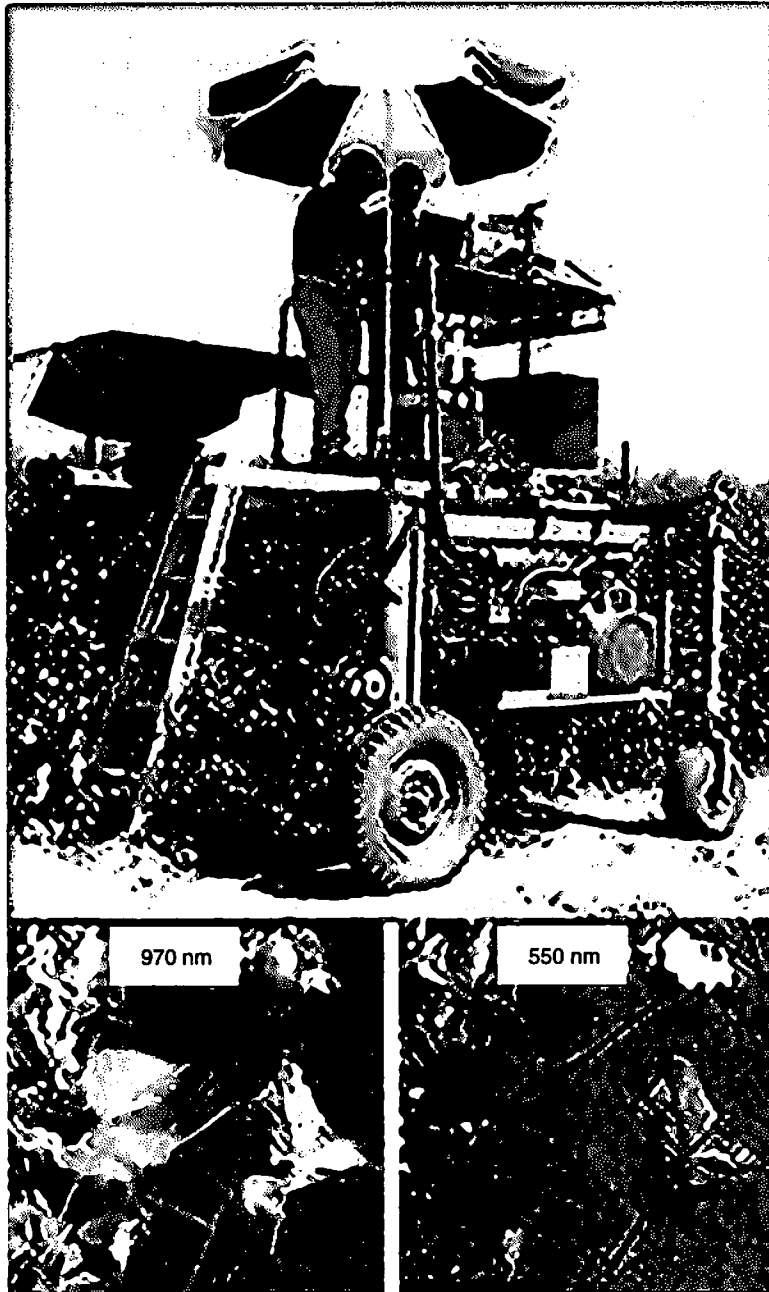


Figure 12.18 Use of a liquid-crystal tunable filter (LCTF) to collect hyperspectral imagery within a cotton field for determining spectral endmembers. The system, mounted on a high-clearance vehicle, is shown at the top, while examples of images of soil and foliage obtained at two different wavelengths are shown at the bottom. See CD-ROM for color image.

bands using this type of system in the field, due to canopy movement in air currents during the measurement.

Use of spectral signatures obtained using an LCTF in performing a linear spectral unmixing of AVIRIS imagery of cotton fields in California was described by Fitzgerald (2000). The procedure was successful in accurately partitioning the image into three endmembers: healthy plant canopy, mite-affected plant canopy, and bare soil. This approach is uniquely different from the image processing examples described earlier, as the source of the spectral signatures (LCTF field measurements) for the three endmembers was independent of the remote sensing image data analyzed using this information.

It is often easy to observe an apparent problem in an agricultural field with basic kinds of remote sensing (like aerial photography) and to use that information to direct a scout into the field to determine the nature of the problem. The current challenge is identification of observed features in remote sensing data to specific crop pests. Results of previous studies suggest that consistent early detection and unambiguous identification of pest effects in remote sensing imagery might ultimately rely on an understanding of how insects and other crop pests specifically affect the remotely sensed characteristics of crops, facilitated in practice by frequent acquisition of high-resolution remote sensing data across a wide range of spectral bands and sophisticated image processing.

12.3.5 Crop Yield

The ability to infer crop yield from remote sensing data has been a goal of agricultural research since the days of planning for the first *Landsat*. Since operational remote sensing systems typically do not have the spatial resolution to count oranges on trees or heads of lettuce in the field, researchers have sought other methods for assessing crop yields from remote sensing data. These methods generally fall into one of the following two categories: (1) reliance on an empirical equation directly relating yield and remote sensing measurements, developed from the results of earlier field studies; and (2) reliance on an established mathematical procedure (possibly an empirical equation or a simulation model) to estimate some characteristic of the crop canopy (such as leaf area index) from remote sensing measurements, which used in turn is in a crop growth model to estimate yield.

12.3.5.1 CORRELATION BETWEEN YIELD AND REMOTE SENSING DATA

Remote sensing researchers have for years observed variations in plant canopy density and condition in high-resolution imagery of agricultural fields and have suspected possible correlations between canopy growth and yield. The recent availability of detailed crop yield maps (Figure 12.19) from yield monitors on harvesting equipment now allows agricultural researchers the opportunity to investigate such correlations in detail. Vellidis et al. (1999) used color and infrared aerial photography to partition the areas of cotton fields into three classes (high, medium, and low yield) that corresponded favorably with data obtained from a yield monitor. They concluded that the highest correlation between their remote sensing data and yield occurred before the cotton canopy covered the soil surface completely. Yang

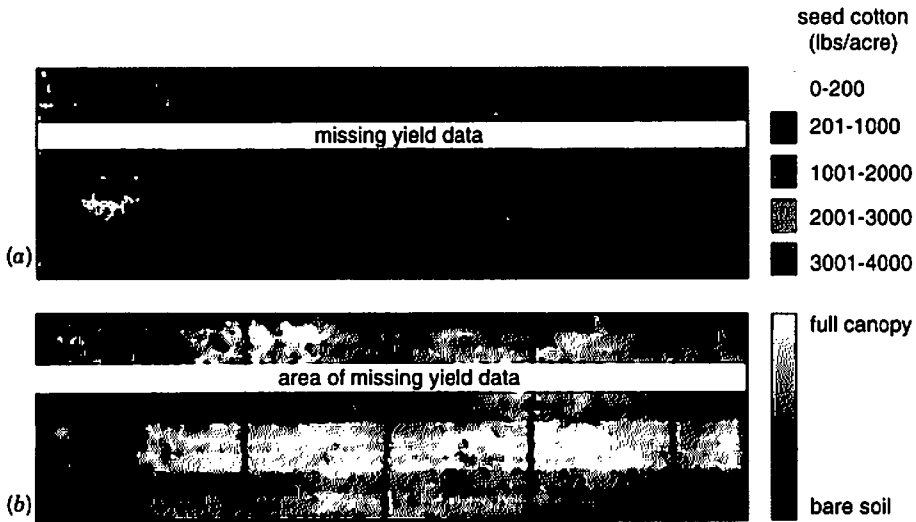


Figure 12.19 Comparison of (a) a cotton yield map obtained at harvest to (b) an aerial infrared image of the field acquired at midseason. Areas in the yield map with very low yield appear to be associated with corresponding areas in the infrared image with reduced ground cover due to insect damage. See CD-ROM for color image.

et al. (1999) found that digitized infrared aerial photographs could be used to partition the area of a grain sorghum field into two to four classes that were similar to patterns observed in yield monitor data obtained for the field. For the case with three classes, analysis appeared to indicate a relationship between class average grain yield and class average image digital count data. Similarly, Fitzgerald et al. (1999c) used high-resolution airborne digital multispectral imagery to partition the area of a sugar beet field into three classes that corresponded favorably with relative variations in root yield across the field, as determined with a yield monitor. For several dates during the growing season, Thomasson et al. (2000) determined the spatial correlation between *Landsat 5 Thematic Mapper* (TM) digital count data and yield monitor data for a cotton field. They observed that the highest correlation involved TM band 4 (NIR) and occurred for an image acquired in late June, approximately 3.5 months before harvest.

These studies suggest that spatial correlations exist between yield and remote sensing data for a number of crops. They also suggest that the significance of these correlations varies over the growing season. Using weekly observations from an airborne digital imaging system, Maas et al. (1999) studied the change in the spatial correlation between yield monitor data and NIR reflectance over the growing season for two irrigated cotton fields. The relationship between yield and reflectance for each image pixel location in one of the fields is shown in Figure 12.20 for three dates during the growing season. Also shown in this figure are the least-squares linear regressions between the yield and reflectance data. The amount of scatter in the points about the regression lines is typical of data derived from yield monitors and high-resolution remote sensing. The change in the statistical significance of this regression over the growing season is shown for this field in Figure 12.21a. The strongest positive correlation between yield and reflectance occurred around mid-

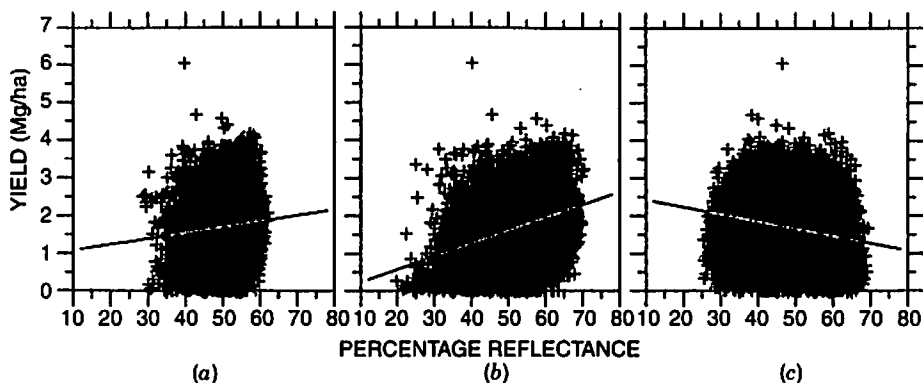


Figure 12.20 Cotton yield at harvest plotted on a pixel-by-pixel basis versus corresponding near-infrared reflectance from imagery acquired on three dates during the growing season: (a) July 14; (b) August 25; (c) September 16. Solid line passing through each cluster of points represents the least-squares linear regression between yield and reflectance. (From Maas et al., 1999.)

season (day 220 to 240), during the period of rapid growth of the cotton bolls. A significant negative correlation between yield and reflectance occurred late in the growing season, prior to defoliation of the crop. This probably resulted from the fact that late in the growing season, cotton plants that bear few mature bolls tend to produce an increased amount of foliage. Results for the second field in this study are presented in Figure 12.21b. For this field, daily irrigation was suspended during two one-week periods during the growing season. The first period, called the *early stress period*, started on day 202. The second period, the *late stress period*, started on day 223. Both stress treatments resulted in observable reductions in NIR reflectance that persisted for approximately two weeks. However, as indicated in the figure, a significant correlation between yield and reflectance occurred only for the

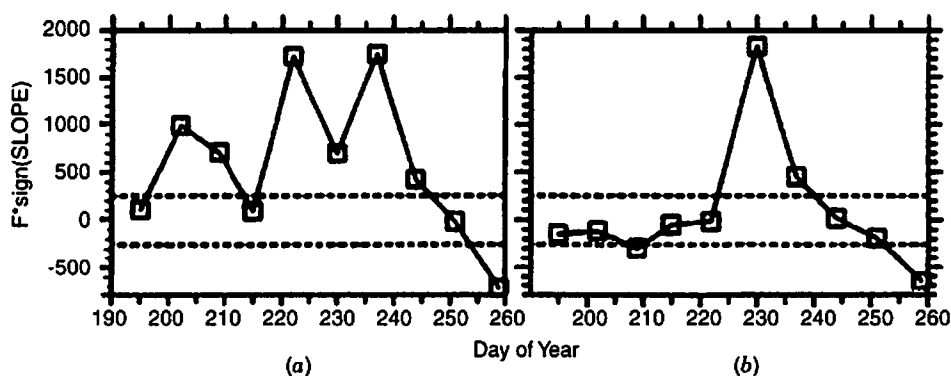


Figure 12.21 Value of the F -statistic times the sign of the slope of the linear regression between yield and near-infrared reflectance plotted versus image acquisition date for two cotton fields. Dashed horizontal lines represent the limiting value of the F -statistic at the 95% confidence level; ordinate values between the pair of horizontal dashed lines in each graph are not significantly different from zero. (From Maas et al., 1999.)

late stress treatment. Of the two treatments, the early stress treatment occurred before the period of rapid boll growth, so the water stress that produced observable effects on the plant canopy did not result in an appreciable reduction in yield.

These results illustrate one of the difficulties in accurately assessing crop yield directly from remote sensing observations. For most crops, a remote sensing observation represents a discrete measurement in time of the state of the crop leaf canopy. Yield observed at the end of the growing season represents an integration of reproductive growth related to the development of the crop leaf canopy over the course of the entire growing season. Due to their timing during the growing season relative to the course of reproductive growth, stress events that might affect the leaf canopy might not appreciably affect yield, as demonstrated by the previous example. Many crop species also have the capacity to compensate for stress-related reductions in potential yield early in the growing season (i.e., wheat plants can compensate for a reduction in the number of panicles early in the growing season by increasing the number of grains produced per panicle later in the growing season).

A second difficulty exists in assessing crop yield directly from remote sensing observations. For most field crops, the plant canopy does not completely cover the soil surface for at least part of the growing season. During this period, remote sensing observations implicitly contain effects related to soil reflectance characteristics (soil background effects). Soil reflectance characteristics are determined by the mineralogical composition of the soil, the amount of organic matter in the soil, the structure of the soil surface, and the amount and type of litter on the soil surface. Thus, remote sensing measurements made at two locations with similar plant canopy characteristics might be different due to differences in soil background effects between the two locations. There have been several attempts to reduce soil background effects in multispectral remote sensing observations through the use of vegetation indexes specifically designed to account for soil reflectance characteristics (e.g., Richardson and Wiegand, 1977; Huete, 1988; Major et al., 1990).

Finally, there is a third difficulty. Remote sensing observations implicitly contain effects related to view angle and scene illumination. For nadir-viewing satellite remote sensing systems, view-angle effects would typically be important only for targets near the edges of regional-scale images. For satellite systems with off-nadir viewing capabilities, such as *SPOT* and *Ikonos*, a field can be imaged on different dates with markedly different view angles. Consider the following example: A field containing row crops with incomplete ground cover might be imaged by a satellite system with a nadir view angle. This image would contain both plant canopy and soil reflectance effects. A day or so later, the same field might be imaged by the same satellite system with an off-nadir view angle. This image could contain fewer soil reflectance effects than the previous image (even though the canopy ground cover had not changed appreciably) as a result of the difference in perspective between the two images.

Difficulties involving view angle become more severe as the observation altitude decreases. View angle and scene illumination effects interact to produce bidirectional reflectance effects (e.g., Jackson et al., 1990). Scene illumination effects are determined by the position of the sun relative to the plant canopy and are related to the latitude, date, and time of day of the observation. Scene illumination effects can be important even for nadir-viewing remote sensing systems. Consider the following example: A field containing crop rows oriented north-south might be imaged by a

remote sensing system with a nadir view angle at approximately local solar noon. In this case, the amount of shadow cast by the crop rows on the intervening soil surface would be minimal. A few hours later, the same field might be imaged by the same remote sensing system in the same manner, but in this case there might be a considerable amount of shadow cast by the crop rows on the intervening soil surface. The average brightness of the field in the second image would be less than the average brightness of the field in the first image, due simply to the presence of more shadow in the second image.

Although differences in scene brightness related to solar altitude and atmospheric clarity can be accounted for through calibration of remote sensing data using reflectance standards (Moran et al., 1997a), there are no simple procedures for removing complex view angle and shadow effects.

The difficulties described above affect the potential accuracy of empirical equations, directly relating yield and remote sensing measurements, because the effects of crop growth stage, soil background, view angle, and scene illumination are implicitly present in the data used to develop the empirical equations. Thus, whereas a significant correlation may be determined within a given data set between crop yield and remote sensing measurements, this relationship will not be unique across locations, dates, and times. Effects like these probably cause the differences noted among empirical relationships developed for a given crop from data sets from multiple sites (Wiegand et al., 1990, 1992; Richardson et al., 1992). These difficulties limit the practical application of empirically derived equations to yield assessment.

Some researchers have sought to improve the accuracy of empirical yield assessment techniques by using successive remote sensing observations to delineate (through interpolation) a remotely sensed surrogate for the seasonal growth curve of the crop canopy. By integrating the area under a portion of this curve representing the portion of the growing season important to yield determination, this procedure attempts to produce a number proportional to the magnitude of the reproductive growth of the crop. This is commonly called the *area under the curve* approach to yield assessment. Thus, Pinter et al. (1981) reported that summing remotely sensed NDVI values from the flowering to mature stages of growth could be used to predict the grain yield of spring wheat. This procedure has been applied to estimating regional wheat yields using AVHRR observations (Doraiswamy and Cook, 1995). Several researchers (Bartholome, 1988; Rasmussen, 1992; Smith et al., 1995a) have reported that accumulated vegetation indexes appear to be a better predictor of crop yields than is a single remote sensing observation.

12.3.5.2 COMBINING REMOTE SENSING WITH CROP GROWTH MODELING FOR YIELD PREDICTION

The elaboration of seasonal growth that results in yield is achieved explicitly by crop growth simulation models. As opposed to remote sensing observations, which are discrete-time events, a growth simulation represents a continuous description of the response of a crop to its environment. Although crop simulation models are based on physiological principles, one must keep in mind that models are only approximations of the actual biological systems that they represent. This fact leads to three operational weaknesses of applying crop growth simulation models:

1. Physiological processes (e.g., photosynthesis, respiration) that determine yield typically appear in models as parameterized representations, so that the accuracy of the growth simulation depend on the particular values ascribed to the parameters in these representations.
2. It is unlikely that the initial or starting conditions for the mathematical representation of crop growth will be known with great certainty for any given field situation.
3. It is unlikely that any given model can adequately incorporate responses to every environmental factor and its possible interactions with other factors that might affect yield for all field situations.

Because remote sensing observations are representative of the actual growth conditions occurring in a field, it was recognized some time ago (Wiegand et al., 1977, 1979; Arkin et al., 1979) that remotely sensed information might be used to improve the accuracy of crop growth simulation models. Early attempts at incorporating remotely sensed information into crop models were reviewed by Maas (1992, pp. 1-3).

Maas (1988a) described and compared four different methods of incorporating remotely sensed information into crop models. Of these methods, reinitialization and reparameterization of the model based on infrequent remote sensing observations were the most effective. *Reinitialization* involves specifying the values of model initial conditions based on comparing the model simulation of a leaf canopy characteristic (such as leaf area index or ground cover) to corresponding estimates of this characteristic determined from remote sensing observations obtained during the growing season. *Reparameterization* is similar, except that model parameter values rather than initial condition are the object of the procedure. Both reinitialization and reparameterization can be used in the same model. An iterative numerical procedure is used to ensure that parameter and/or initial condition values are selected, so that following convergence, the model simulation agrees with what is observed in the field. Since the data for adjusting parameter and/or initial conditions are observed during the growing season for which the simulation is being made, this procedure has been called *within-season calibration* of models. This process has been described in detail by Maas (1988a, 1992, 1993a) and is shown diagrammatically in Figure 12.22.

Within-season calibration acts to ameliorate the three operational weaknesses listed above for crop growth simulation models. This procedure results in the objective selection of parameter and/or initial condition values that lead to agreement between the model simulation and observed field conditions. Through what has been called the *folding-in phenomenon*, the effects of environmental factors that are not explicitly incorporated into the model formulation will be implicitly incorporated into the model simulation when the values of existing parameters and/or initial conditions are adjusted by the within-season calibration procedure.

Maas (1988b) demonstrated that model reinitialization based on satellite-derived estimates of leaf area index improved the average yield estimate for 37 grain sorghum fields in South Texas from a 30% underestimate to a 2% overestimate of the observed value. Reinitialization and reparameterization of a model using *Landsat* data resulted in an average yield estimate within 5% of the observed value for 115 spring wheat fields in North Dakota (Maas, 1991). Similar calibration of a model

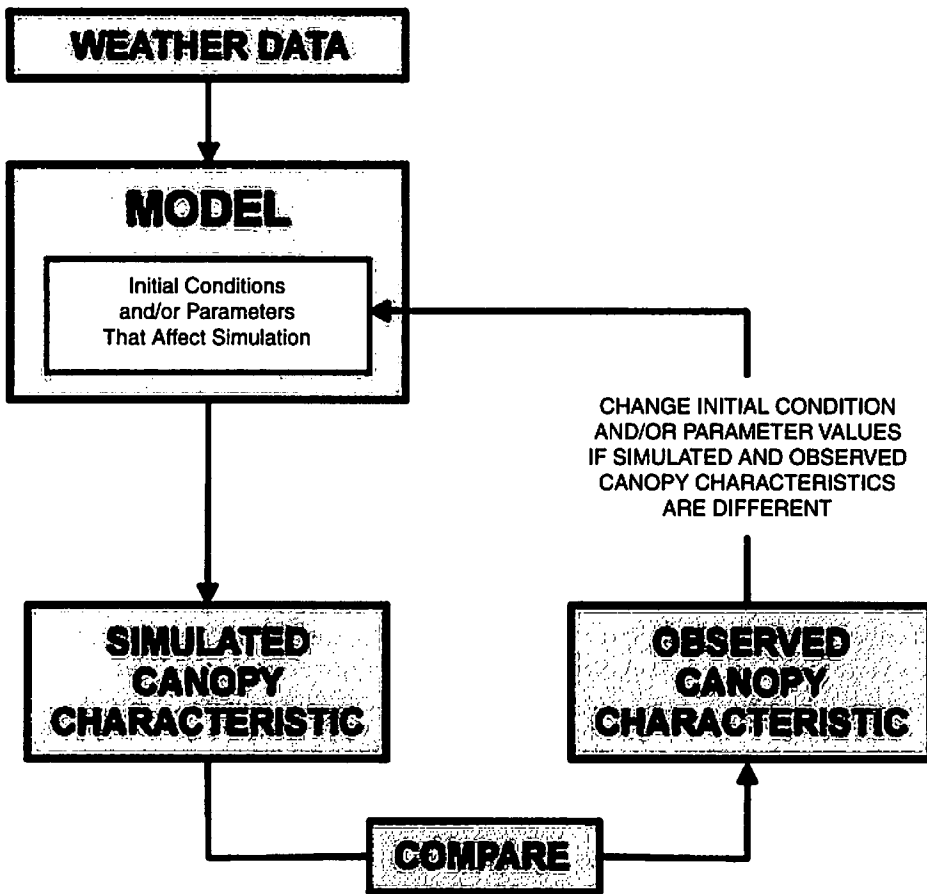


Figure 12.22 Within-season model calibration procedure.

using ground-based canopy reflectance measurements resulted in an average yield estimate within 6% of the observed value for 52 winter wheat research plots at three locations in the U.S. Great Plains (Maas, 1993b).

In these examples, leaf area index values were estimated from remote sensing data using empirically derived relationships. Doraiswamy et al. (2000) has recently reported on the use of the SAIL radiative transfer model to estimate leaf area index values from remote sensing data and the use of these values in a within-season calibration of a version of the EPIC model to determine regional crop yields. This combination of approaches minimizes reliance on empirical procedures, thus increasing its general applicability across locations, dates, and times. Maas (2000) has described the inclusion of a program module into crop growth models to explicitly simulate scene reflectance based on modeled plant canopy architecture, known leaf and soil reflectance characteristics, and ambient illumination conditions. This would allow direct comparison of simulated scene reflectance with remote sensing observations to facilitate the within-season calibration of the models (see Jacquemond et al., 2000).

An additional advantage of the use of crop growth models in assessing yield is that they can be used to predict yield objectively prior to the end of the growing season. This can be accomplished using the following procedure. During the growing season, the crop model can be run from the start of the season to the current date using observed weather data, and can be calibrated using available remote sensing observations as described above. For the remainder of the growing season, computer-generated (synthetic) weather data (e.g., Richardson, 1981; Richardson and Wright, 1984; Hanson et al., 1994) can be used to complete the model simulation of crop growth and yield. Due to the uncertainty of future weather conditions, the model should be run using a large number of different years of synthetic weather data. The model will produce a yield prediction for each year of synthetic weather data. The distribution of these predicted yields can then be analyzed statistically to produce a probabilistic prediction of yield for the current year. This probabilistic prediction will be the probability (or chance) that the yield at harvest will be within a certain range, or will be greater or less than a certain value. The certainty of this prediction should increase over the course of the growing season as the model simulations of crop growth become based more on observed weather conditions and remote sensing data and less on synthetic weather data.

Traditionally, crop growth models have been designed to simulate an "average" plant within a given area such as a field. Thus, they cannot directly provide information on the spatial variability of crop growth and yield within the given area. By converting remote sensing imagery into spatial arrays of crop canopy characteristics (such as leaf area index or ground cover) for use in within-season calibration, crop models can be used to explicitly generate spatial distributions of yield within a given area of interest, such as a field. Alternatively, remote sensing imagery can be used to partition areas such as fields into portions (commonly called *production zones*) with similar characteristics for which the models can be run. The unique temporal qualities of models and spatial qualities of remote sensing make the combination of these technologies particularly attractive to modern agricultural applications such as precision farming.

12.3.6 Soil Characterization

In irrigated agriculture, the level of many input requirements is dependent on soil characteristics such as water-holding capacity, organic matter content, and salinity levels. Knowledge of water-holding capacity is critical to good irrigation management, organic matter content affects the rate of application of fertilizers and pesticides, and soil salinity levels can have large impacts on crop yield. Because soil properties are very important to management decisions and the soil often determines the yield potential of a given area, soil mapping was one of the first applications of remotely sensed data for agriculture (Bushnell, 1932). Aerial photographs have been used as a mapping aid in most soil surveys in the United States since the late 1950s. The new tools of variable-rate application and global positioning systems have generated a need for high-spatial-resolution soil maps. Often, these maps are created from samples collected on a fixed grid, with statistical interpolation between sample points (Nielsen et al., 1995); however, the expense of collecting and analyzing the number of samples can sometimes become economically prohibitive (Ferguson et

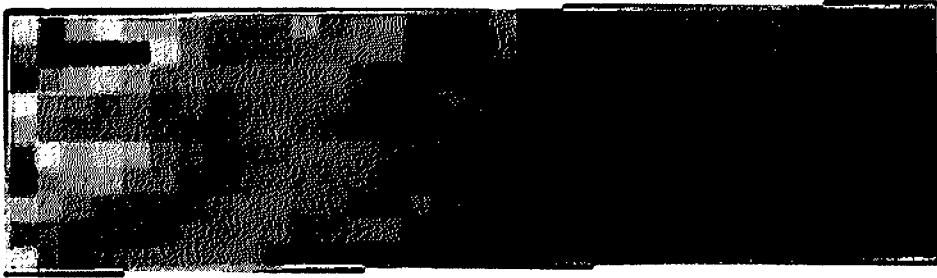
al., 1996). Therefore, even more emphasis is now being placed on the use of remotely sensed data to quantify differences in soil physical properties.

Quantitative relationships have been developed between reflectance data and soil properties using prepared soil samples under controlled conditions. Post et al. (2000) found that broadband soil albedo (0.3 to 2.8 μm) could be predicted accurately from reflectance measurements in the NIR, blue, and green spectral regions. Stoner and Baumgardner (1981) examined 485 uniformly moist soil samples in the laboratory and determined that five characteristic reflectance spectra (0.52 to 2.32 μm) were present that could be related to differences in organic matter content, iron content, and texture. Other soil properties have been inferred from reflectance measurements under laboratory conditions such as moisture, organic carbon, and total nitrogen (Dalal and Henry, 1986; Shonk et al., 1991), as well as other chemical properties (Ben-Dor and Banin, 1994).

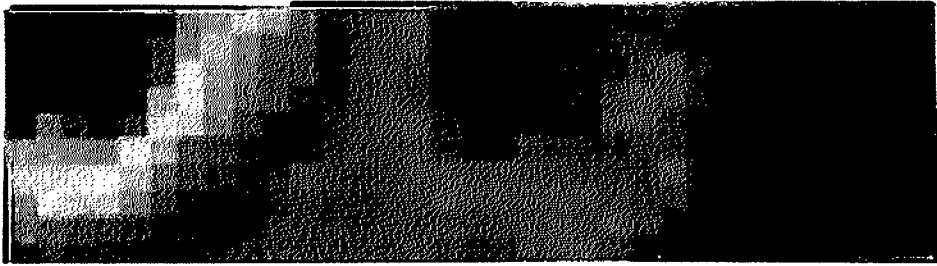
Even though strong correlations between reflectance data and soil properties have been found in a laboratory setting, extracting similar information from imagery of tilled fields can be more challenging. First, if a soil properties map for use in agricultural management decisions is derived from reflectance or emitted thermal data, an implicit assumption is that the soil properties at the surface correlate to changes throughout the root zone. Second, changes in surface tillage condition (e.g., bedded vs. flat, fine disking vs. coarse plow), rain compaction, moisture, and plant residue all may induce changes in apparent soil reflectance that approach or exceed spectral responses, due to physical soil properties such as texture and organic matter (Barnes and Baker, 2000; Courault et al., 1993). For example, Matthias et al. (2000) found the broadband albedo (0.3 to 2.8 μm) of a moldboard-plowed soil surface was reduced by 27% compared to the same soil passed through a 2-mm sieve and smoothed with a straightedge. Wet soils can have a decrease in visible and NIR reflectance by as much as 25% from a dry condition, and these changes are not always consistent between wavelengths (Bedidi et al., 1992). Despite these limitations, bare soil imagery has been used successfully to characterize soil properties, particularly when the analysis is conducted over a limited geographic area and the areas considered have similar surface conditions. Examples of the use of remotely sensed data for soil characterization from the literature are discussed in the following paragraphs for soil properties that are particularly important to irrigated agriculture.

12.3.6.1 SOIL TEXTURE AND WATER-HOLDING CAPACITY

Farm managers and consultants often use a soil water balance to determine irrigation schedules. A key input to the water balance equation is the amount of water that can be stored in the soil's root zone. The water-holding capacity of a soil is closely related to the soil's particle size distribution, and thus various models have been developed to relate soil water holding capacity from soil textural information (e.g., Schaap et al., 1998; Arya et al., 1999). Reflectance measurements over tilled fields have been used with varying levels of success to develop predictive equations for the fraction of sand, silt, and/or clay at the soil surface (Suliman and Post, 1988; Coleman et al., 1991). An example relationship between NIR imagery and sand content is presented in Figure 12.23 for data collected in an agricultural field near Shafter, California. The soil brightness map derived from a NIR image of a field is shown at the top of the figure, and a soil texture map interpolated from grid sam-



(a)



(b)

Figure 12.23 (a) Soil brightness map derived from NIR data and (b) soil texture map created from interpolated grid samples (bottom) for an agricultural field near Shafter, California. See CD-ROM for color image.

pling for the same field is shown at the bottom. These maps have been scaled similarly so that the resulting values range from 0 to 255, and then assigned the same pseudocolors. Figure 12.24 shows the correlation between soil texture (sand content) and remotely sensed soil brightness. This correlation could be used to derive a detailed soil surface texture map from a NIR image when calibrated from a limited number of samples. Dependable relationships such as the one in this example are only possible when imagery is acquired over fields with uniform tillage conditions (Barnes and Baker, 2000). To minimize the effects of soil properties other than texture (e.g., soil moisture, organic matter, minerals other than quartz), Salisbury and D'Aria (1992) used a combination of visible, NIR, and TIR data. The increased availability of hyperspectral data, particularly in the SWIR spectral region around 2.3 μm , has introduced the potential to discriminate between different types of clays, such as kaolinite and smectite (Chabrilat et al., 1997; Drake et al., 1999). This has agricultural significance, as clay mineralogy has a large impact on the soil's ability to store and hold nutrients, and its physical reaction to tillage operations. Increased spectral resolution may also improve the ability to detect differences between closely related soil types. For example, Palacios-Orueta and Ustin (1996) found that multivariate analysis techniques applied to AVIRIS data provide the ability to identify differences between soil mapping units that were from the same soil series.

Patterns in soil surface color and crop development have also been associated with the water-holding capacity of the soil (Milfred and Kiefer, 1976; Wildman, 1982). Wildman (1982) found that patterns in aerial photographs of grape vines

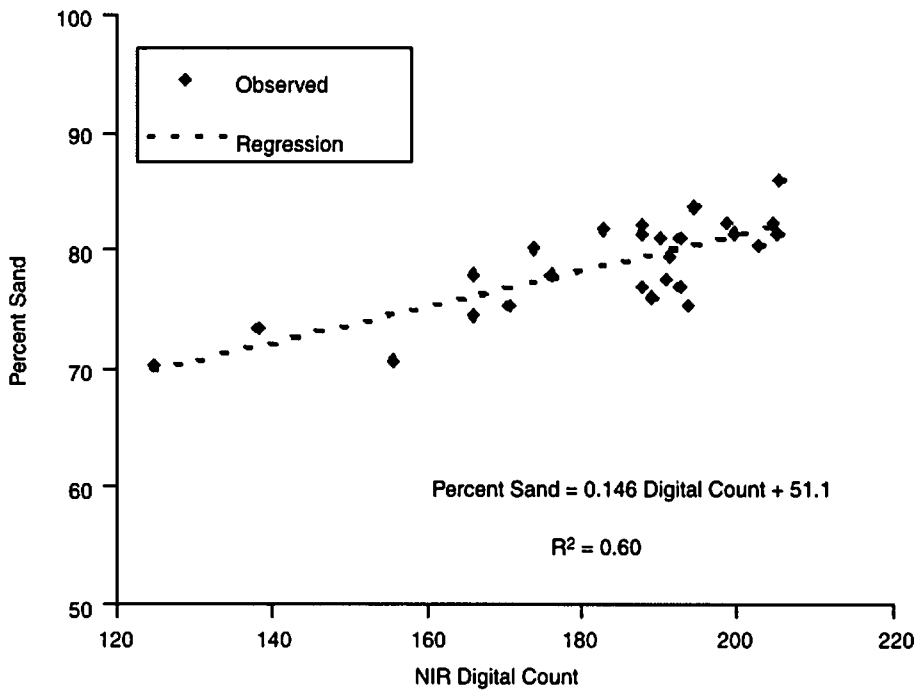


Figure 12.24 Percent sand versus NIR digital count for data from the images in Figure 12.23.

could be related to differences in soil texture, which in turn affected the soil water-holding capacity. Some caution must be exercised in interpreting cropping patterns in this manner, as the lack of irrigation uniformity can sometimes add a source of crop growth variability beyond that of soil properties (Adamsen et al., 2000).

12.3.6.2 SOIL ORGANIC MATTER

Soil organic matter content is an important consideration in many procedures to determine the rate at which various agricultural inputs are applied. For example, the application rate of some herbicides increases with increasing organic matter, whereas nitrogen requirements can decrease with increasing organic matter (Sudduth et al., 1997). Soil organic matter has been related to reflectance data collected over agricultural fields in several studies (e.g., Coleman et al., 1991; Henderson et al., 1992; Chen et al., 2000). Henderson et al. (1992) examined the correlation between soil organic matter content and reflectance between 0.4 and 2.5 μm at 0.01- μm intervals. They found that visible wavelengths (0.425 to 0.695 μm) had a strong correlation with soil organic matter (an r value of at least -0.991) for soils with the same parent material; however, the relationship was very sensitive to Fe and Mn oxides for soils from different parent materials. Use of middle-infrared bands improved predictions of organic carbon content when the soils were from different parent materials. As the visible spectrum can be correlated with organic matter in soils of the same parent material, it may be possible to predict within-field variations in organic matter from locally derived relationships and true color imagery (Chen et al., 2000). In circumstances where differences in iron content may influence the

accuracy of organic matter prediction from spectral data, Palacios-Orueta and Ustin (1998) found that principal component analysis of AVIRIS data could be used to extract information on both properties.

12.3.6.3 SOIL SALINITY

An increase in soil salinity can be detrimental to crop growth and yield; however, management practices are available to allow saline soils to maintain productivity (Hoffman et al., 1990). Remotely sensed data have been used to identify salt-affected soils so that appropriate management actions can be taken (Verma et al., 1994; Wiegand et al., 1994). Many salt-affected soils can be identified by a white salt crust that forms on the soil surface; thus these soils tend to have higher visible and NIR reflectance (Rao et al., 1995). This spectral response cannot always be used to identify saline soils, as in some geographic locations, soils with high sand contents will have visible and NIR spectral properties similar to salt-crust soils (Verma et al., 1994). The ability to discriminate salt-affected soils has been improved through the inclusion of thermal data (Verma et al., 1994) and L-band microwave data (Sreenivas et al., 1995). Kluitenberg and Biggar (1992) found that thermal data could detect differences in canopy temperature that were induced by different soil salinity levels when the field was recently irrigated. Dependable differentiation of salinity problems was less effective as time from the last irrigation increased. Patterns in vegetation development over fields with known salinity problems can also be used to map soil salinity levels through the use of vegetation indexes (Wiegand et al., 1994). The accuracy of estimates of saline areas based on vegetative spectral response may be limited when there are other factors affecting the crop's development (Wiegand et al., 1997). To minimize confounding factors due to crop stress other than salinity, Mikati and Neale (1997) used a model that first classified crop areas into stressed and nonstressed areas using visible and NIR infrared data. The model then used thermal data to distinguish between nutrient and salinity stress, as nutrient stress does not affect canopy temperature as strongly as does salinity.

12.3.6.4 OTHER APPROACHES TO CHARACTERIZE SOIL PROPERTIES IN IRRIGATED AGRICULTURE

Rather than relying on a specific spectral response to a particular soil property, the concept of *directed soil sampling* has been developed (Pocknee et al., 1996). The idea is first to acquire imagery of a bare soil field and then take soil samples from areas in the image with distinct spectral features. Correlations or classification schemes are then developed between the spectral classes or reflectance levels and soil properties of interest. Pocknee et al. (1996) found that this method worked well for mapping soil phosphorus, but performed poorly for soil pH. Directed soil sampling can often provide soil maps of similar or better accuracy to those derived from interpolation techniques such as kriging or distance-weighted interpolation with fewer soil samples (Thompson and Robert, 1995; Barnes and Baker, 2000). A similar approach can be used over fields with a crop present by collecting soil samples and plant material for analysis over areas with similar spectral classes (Yang and Anderson, 1996).

Other opportunities are emerging that could potentially improve the ability to characterize soil properties from remotely sensed data. Progress made to estimate plant litter levels from remotely sensed data (e.g., Nagler et al., 2000) is one example

of additional data processing that may ultimately result in better estimates of soil properties. With more robust estimates of litter, this source of variation can be eliminated from scenes of fallow fields, increasing the correlation between the remaining reflectance variations in the scene with soil properties. Sudduth et al. (1997) review various ground-based sensor systems that have been used to rapidly assess spatial variability in selected soil properties. These systems include electromagnetic induction measurements (correlated to soil texture, moisture content, salinity, topsoil depth), contact soil electrode probes mounted on agricultural implements (soil salinity and pH), and the use of fiber optics attached to tillage implements to acquire subsurface soil spectra. Integration of these data with imagery and other ancillary data could ultimately lead to algorithms that are more dependable and require less local calibration for soil characterization. Sommer et al. (1998) provide examples of different frameworks used to integrate multispectral imagery with various ancillary data sources.

12.3.7 Next-Season Preparation

Strong relationships have been demonstrated between terrain and biogeophysical processes and characteristics. Soil properties, land cover types, and surface topography combine to drive the physical processes controlling infiltration, excess rainfall generation, and runoff, which in turn directly affect soil moisture and influence the spatial variability of crop production. These processes also affect water quality and sediment discharge through the erosion of surface soil and removal of fertilizers and pesticides. Effective next-season preparation relies on the assessment of a field's physical processes to promote improved planning for the upcoming season, and terrain models offer promise in the improved representation of the physical characteristics of the field.

A significant growth area in the field of precision agriculture is the linkage of predictive models for hydrology, soil moisture, and erosion with farming practices to improve management and yield. Such models require detailed spatially distributed information, information that may be attained remotely on an annual basis to update and improve such models' predictive capabilities. High-resolution terrain mapping can also be used to assess surface changes that have occurred since the previous measurement and identify problem areas for runoff, erosion, and soil moisture.

In the interval between harvest and planting, a digital elevation model (DEM) may be created for the purpose of isolating areas that have undergone significant change since the last observation. Planning and preparation for the next season can be better suited for erosion control practices through the application of predictive models. Models such as the revised universal soil loss equation (RUSLE) (Renard et al., 1997), the kinematic runoff and erosion model (KINEROS) (Smith et al., 1995b), and the Water Erosion Prediction Project (WEPP) (Lane et al., 1992) recognize the strong relationship among soil slope, runoff, and erosion. The control and reduction of surface runoff is important in irrigated agriculture to optimize the application of water to both limit off-site impacts and control soil moisture. Infiltration processes are inextricably linked to runoff and soil moisture, and the assessment of surface topography and use of physically based models can aid in

next-season preparation to maximize the relationship between irrigation application and soil moisture.

The integration of terrain modeling with preseason field preparation can improve annual yield, reduce off-site impacts, and be of monetary benefit due to the improvement in long-term stability of the field and reduced costs associated with erosion and the misapplication of water, nutrients, and pesticides. However, the effective use of terrain models for field preparation necessitates a highly accurate representation of topography since even relatively small errors can lead to wide variations in change detection and prediction of field response to management practices. Commonly available digital elevation models (DEMs) such as the U.S. Geological Survey 7.5-minute topographic maps are inadequate for field preparation both spatially, since they have a 30-m resolution with up to 1/2 contour vertical error (USGS, 2000), and temporally, since they are formed from outdated photography.

Recent innovations in the use of interferometric synthetic aperture radar (IFSAR) and laser-induced detection and ranging (lidar) have offered avenues toward the rapid and accurate creation of DEMs for intercrop landscape assessment. These evolving tools rely on active remote sensing platforms to form a detailed depiction of land surface by sending a signal from the platform (either airborne or satellite) and decoding the complex signal that returns to the sensor. Lidar has the capacity to resolve finer details of the land surface than does IFSAR, but IFSAR is more suitable for mapping large, spatially complex areas. Custom DEMs are often made using stereo photography, and such techniques can be highly accurate. However, both IFSAR and lidar are more rapidly acquired and offer higher vertical accuracies than do traditional stereo photographic techniques.

12.3.7.1 INTERFEROMETRIC SYNTHETIC APERTURE RADAR FOR CREATING DEMS

Terrain mapping with synthetic aperture radar involves decoding the complex interaction of multiple images taken from either an airplane or a satellite platform. Interferometric mapping is used to create DEMs, wherein images are taken of the same location either at different times or from different locations. The resultant images “interfere” with one another to create a three-dimensional portrait of the target area. In *single-pass interferometry*, two sensors are mounted on a single platform (i.e., an airplane) and both sensors target the same location. In *repeat-pass interferometry*, the same sensor is passed over the target location after a given period of time. In the first case the baseline separation that allows for the images to be interfered is spatial, whereas in repeat-pass interferometry, the baseline separation is temporal.

Imaging radar has been used to estimate surface height since at least the early 1970s (Graham, 1974). A detailed technical discussion of IFSAR is beyond the scope of this review; for more information the reader is referred to Rany (1999). A schematic representing the case of single-pass interferometry is shown as Figure 12.25. In this example, an airplane is outfitted with two radar sensors that continually emit pulses perpendicular to the flight track. In this arrangement the spatial baseline is known; thus measurement of the azimuthal angle, range, and elevation angle allow for the absolute determination of the vertical distance to the object. With detailed

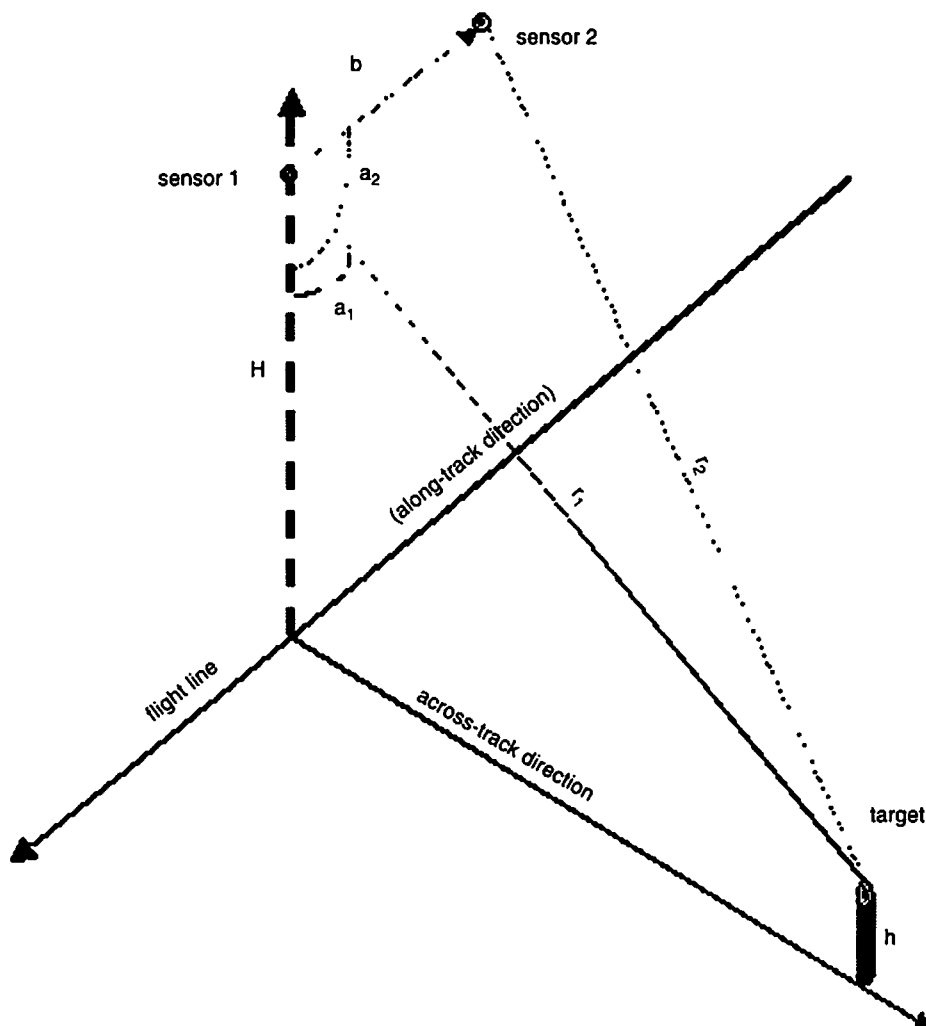


Figure 12.25 Single-pass interferometric SAR system. Two sensors target the same object on the ground perpendicular to the flight path. The spatial baseline (b) between the sensors and the geometric configuration [i.e., sensor height (H), imaging angles (α_1 and α_2) are known]. Given the path lengths of r_1 and r_2 as well as phase differences in the signals, the solution for the target height (h) can be determined.

knowledge of the imaging platform's flying height provided by differential global positioning systems, the image area can be geo-rectified to Earth's surface.

Commercially available satellite and airborne IFSAR products offer a range in cell resolution and sensor type. Table 12.4 details the specifications of selected commercially available IFSAR platforms. Note the high spatial resolution offered by many of these systems. The spatial resolution and vertical accuracies of IFSAR platforms lend themselves well to surface observations. For example, accuracies of 1 m in flat regions have been found by Madsen et al. (1995) using TOPSAR data; Gabriel et al. (1989) used *Seasat* data to produce DEMs with 10 m resolution to detect

TABLE 12.4 Examples of Commercially Available IFSAR Systems

<i>IFSAR System</i>	<i>Platform^a</i>	<i>Frequency (GHz)</i>	<i>Look Angles (deg)</i>	<i>Baseline Length (m)</i>
TOPSAR	Airborne	5.3	30–55	2.5
INSAR	Airborne	5.3	30–55	2.8
STAR-3i	Airborne	10	3–60	1
SRTM	Shuttle	5.6, 10	52	60
SEASAT	Satellite	1.275	20–26	4500
ERS-1	Satellite	5.3	21–26	1115
JERS-1	Satellite	1.275	35	4500

^aThe airborne platforms are single-pass systems, whereas the satellite platforms are repeat-pass.

changes on the order of 1 cm. Izenberg et al. (1996) were able to use SIR-C and TOPSAR data to detect small changes in elevation resulting from flood-caused erosion and deposition on agricultural fields.

12.3.7.2 LIGHT DETECTION AND RANGING FOR CREATING DEMS

Laser-induced detection and ranging (lidar) is, like IFSAR, an active remote sensing system. A laser rangefinder mounted on an aircraft emits a continual stream of pulses to record a swath of data (Krabill et al., 1984). Since the speed of the laser pulse and the angle of orientation are known, the time of return is used to calculate the distance from the aircraft to the ground. Laser pulses, being of extremely high frequency, are reflected by objects targeted on the ground and penetrate vegetation and soil considerably less than do the longer-wavelength SAR signals.

Similar to IFSAR, it is critical that the absolute location of a laser rangefinder be known to generate an accurate depiction of Earth's surface. Toward that end, the aircraft is outfitted with a differential global positioning system and complex inertial reference systems to measure the location and orientation of the sensor platform. These measurements are integrated into the postprocessing of the laser return data to develop a georeferenced portrayal of the targeted terrain. Elevation estimates from airborne laser altimeters can be highly accurate, with correspondingly detailed resolution. Ritchie et al. (1993) reported absolute vertical accuracies of 0.05 m with 0.015 to 0.02-m spatial resolution; Marks and Bates (2000) used a lidar DEM with 3 m spatial resolution with 0.01 to 0.015 m of vertical accuracy in floodplain mapping for hydrologic modeling.

Limitations in the efficacy of IFSAR and lidar for terrain modeling are present, and some caveats regarding their use are warranted. First, since SAR images are coherent, the phase of the signal is retained and used in the determination of topographic height. Difficulties arise in devolving phase information in regions of rapidly changing relief such as escarpments. In this case the two sensors may receive signals with phase differences greater than 2π , due to the steep slope, exceeding the detectable differences in phase and necessitating phase-unraveling algorithms. Second, both IFSAR and lidar accuracies are reduced by vegetation, since leaves, branches, and stems can either partially or totally reflect their signals, causing confusion and introducing error to the elevation estimate. Third, laser and radar signals

penetrate the soil surface to a depth dependent on their wavelength, soil type and structure, and soil moisture. Fortunately, the impacts of each of these factors are reduced when they are employed in agricultural next-season preparation. Low slopes and relatively homogeneous soils typify agricultural fields, and soil moisture may be controlled in advance of a DEM mission to reduce confounding effects.

Both IFSAR and lidar applications are considered emerging technologies in the field of irrigated agriculture. As precision farming practices evolve, the integration of detailed spatial data with physically based predictive models and improved farming practices may serve to improve yield and the long-term sustainability of farmlands. High-resolution DEMs from these remote sensing platforms may be used in next-season preparation to detail changes in the land surface resulting from the preceding period's farming practices. They may also be tied to predictive models to optimize irrigation practices with respect to soil moisture and investigate improved farming practices to mitigate the effects of runoff and erosion.

12.4 CONCLUSIONS

This chapter offers numerous remote sensing products in response to seven of the nine information needs identified by corn, cotton, soybean, and wheat growers (Table 12.1). The most mature products, models, and sensor systems are available for monitoring and predicting crop yield and crop water status. A measure of success in these areas is the commercial development of the CWSI and TKW concept and the implementation of remote sensing approaches for operational international crop yield assessment by the U.S. Foreign Agricultural Service. These successes are the result of focused remote sensing research on crop water stress and crop yield based on field studies conducted for many decades, especially through the LACIE, AgRISTARS, and NASA-funded *Landsat* research.

Opportunities for deriving crop nutrient status and weed infestation from remote sensing have recently increased with the development of new hyperspectral and narrowband multispectral imaging sensors. Many of the approaches for detecting nitrogen deficiencies are based on the absorption of light in narrow wavebands associated with leaf chlorophyll content. Image-based analysis techniques capable of quantifying the location and magnitude of within-field nutrient deficiencies are under very active investigation. Similarly, weed infestations are often based on detecting differences in the spectral signatures of crops and weeds, requiring a hyperspectral measurement. However, at present there are no robust, widely available, consensus-driven methodologies for remotely sensing nitrogen deficiencies or weed infestations in crop canopies imaged at any scale.

The production of fine-resolution DEMs with high vertical accuracies has become operational in the last decade with the development of airborne imaging IFSAR and lidar systems. The recent NASA *Shuttle Radar Topography Mission* (SRTM) demonstrated the technical feasibility of large-scale imaging radar for topography. In the year 2000, approximately 80% of Earth's land mass was mapped in just over 11 days with a spatial resolution of 30 m and a 10-m maximum relative height accuracy (NASA, 2001) to meet Interferometric Terrain Height Data (IHTD)-2 specifications. Such coverage and accuracy should be useful as supplemental information for the

management of large agricultural areas and underscores the emerging technical capabilities associated with IFSAR.

It has been more difficult to derive information about soil properties from spectral data because remote sensors provide only a surface measurement, and changes in the soil surface condition and vegetation cover mask spectral responses due to soil properties. However, success has been achieved under controlled conditions or over limited geographic areas. Remote sensing for monitoring insect infestations has been limited largely to after-the-fact insect damage assessment, but recent development and launches of multispectral sensors with fine resolution have stimulated efforts to observe the early stages of pest infestations and areas with potential for pest infestation in time for control measures.

For each management information need identified in Table 12.1, there are examples of products that can be derived from imaging systems with wide visible, NIR, and TIR spectral bands. The *Landsat*-like spectral bands have been the workhorse for agricultural remote sensing for the past 25 years and will probably continue in that role with the recent successful launch of the *Landsat 7 Enhanced Thematic Mapper* (ETM+). However, exciting new technologies for providing crop condition information were also reported in this chapter, including biochemical analysis for monitoring crop water stress, shape analysis for weed detection, linear spectral unmixing for insect detection, combined remote sensing/modeling approaches for crop yield, red-edge analysis for determining crop nutrient and water status, data fusion of optical and radar measurements to map soil properties, and use of IFSAR and lidar for digital terrain modeling. The technologies of the future will probably include sensors to measure natural and genetically induced fluorescence related to crop vigor (e.g., Chappelle et al., 1984; Liu et al., 1997), more focus on multispectral data fusion and multidomain indices (e.g., Clarke et al., 2001), and increased use of remotely sensed data as an integral part of agricultural decision support systems (e.g., Sommer et al., 1998).

Approaches reported here based on surface reflectance and temperature suffered from common limitations, including image degradation due to variations in atmospheric optical depth, clouds, sun-sensor-surface geometry, and sensor and platform limitations (e.g., coarse spectral and spatial resolutions, slow image turnaround times, and infrequent repeat coverage). Because of these, many studies have been conducted with handheld sensors at the field-plot scale. On the other hand, advances in sensor design and image processing have addressed, and in some cases overcome, these limitations. Such advances include image postprocessing models, designed to minimize effects of sensor geometry and atmospheric variations, platform improvements to improve image turnaround and repeat coverage, and sensors designed for the highest possible spectral and spatial resolutions and coverage. In contrast, approaches for deriving DEM products from active radar and laser signals have circumvented most of the above-mentioned problems associated with optical sensors. Furthermore, DEMs can be produced between growing seasons, thus avoiding the frustrations of inadequate image turnaround and repeat coverage.

The sensor and platform technology to provide spectral imagery suitable for nearly all the applications presented in this chapter is currently available and largely tested in orbiting systems, but a single system dedicated to agricultural management does not exist (Moran, 2000). When the system specifications for an orbiting agri-

cultural sensor are defined and the sensor is built and launched, the real information needs of farm managers can be met by remote sensing.

12.5 ACKNOWLEDGMENTS

The authors would like to thank Chandra Holifield for her help with library searches on several topics. Also, thanks go to Pamela K. Russ and James S. Tillman, library personnel at the University of Florida Citrus Research and Education Center, Lake Alfred, Florida.